The Whole Antarctic Ocean Model (WAOM v1.0): Development and Evaluation

Ole Richter[1,2], David E. Gwyther[1], Benjamin K. Galton-Fenzi[3], and Kaitlin A. Naughten[4]

[1]Institute for Marine and Antarctic Studies, University of Tasmania, Private Bag 129, Hobart, TAS, 7001, Australia.
[2]Geography & Spatial Sciences, School of Technology, Environments and Design, University of Tasmania, Hobart, TAS, 7001, Australia.
[3]Australian Antarctic Division, Kingston, TAS, 7050, Australia.
[4]British Antarctic Survey, High Cross, Madingley Road, Cambridge, CB3 0ET, United Kingdom.

Correspondence: Ole Richter (ole.richter@utas.edu.au)

Abstract. The Regional Ocean Modeling System (ROMS), including an ice shelf component, has been applied on a circum-Antarctic domain to derive estimates of ice shelf basal melting. Significant improvements made compared to previous models of this scale are the inclusion of tides and a horizontal spatial resolution of 2 km, which is sufficient to resolve onshelf heat transport by bathymetric troughs and eddy scale circulation. We run the model with ocean-atmosphere-sea ice conditions from
5   the year 2007, to represent nominal present day climate. We force the ocean surface with buoyancy fluxes derived from sea ice concentration observations and wind stress from ERA-Interim atmospheric reanalysis. At the northern boundaries ocean conditions are derived from the ECCO2 reanalysis and tides are incorporated as sea surface height and barotropic currents. The accuracy of tidal height signals close to the coast is comparable to those simulated from widely-used barotropic tide models, while off-shelf hydrography agrees well with the Southern Ocean State Estimate (SOSE) model. On the shelf, most details of
10 ice shelf-ocean interaction are consistent with results from regional modelling and observational studies, although a paucity of observational data (particularly taken during 2007) prohibits a full verification. We conclude that our improved model is well suited to derive a new estimate of present day Antarctic ice shelf melting at high resolution and is able to quantify its sensitivity to tides.

15 # 1 Introduction

Modelling of Antarctic ice shelf-ocean interaction is critical to predicting future changes in sea level and climate. Antarctic glaciers drain into floating ice shelves and melting or marine ice accretion at the base of these ice shelves changes their ability to buttress inland ice sheet discharge (e.g. Dupont and Alley, 2005; Gudmundsson, 2013; Pritchard et al., 2012). In turn, glacial melt water impacts the surrounding oceans with consequences for global ocean circulation and climate (e.g. Jacobs,
20 2004; Purkey and Johnson, 2013). Ocean models that include an ice shelf component are playing a key role in estimating

the current state of ocean-ice shelf interaction (e.g. Galton-Fenzi et al., 2012; Gwyther et al., 2014; Hattermann et al., 2014), understanding the underlying mechanisms of ice shelf melting (e.g Makinson et al., 2011; Hattermann, 2018; Gwyther et al., 2018) and predicting future changes (Kusahara and Hasumi, 2013; Mueller et al., 2018; Naughten et al., 2018a). Within these models, Antarctic-wide applications are of particular interest, as they resolve ice shelf teleconnections (Gwyther et al., 2014;
25 Silvano et al., 2018) and smaller ice shelves with less research focus, all around the continent (Timmermann et al., 2012). Further, consistent model design and parameter choices in large scale models make it easier to compare different regions, and coupled ice sheet-ocean models for climate predictions will ultimately need Antarctic-wide domains (Asay-Davis et al., 2017).

The accuracy of circum-Antarctic ocean-ice shelf models, however, suffers from incomplete model dynamics and poorly represented subgrid scale processes. Many ocean models with pan-Antarctic coverage have now been augmented by an ice
30 shelf component (e.g. Hellmer, 2004; Timmermann et al., 2012; Kusahara and Hasumi, 2013; Dinniman et al., 2015; Schodlok et al., 2016; Mathiot et al., 2017; Naughten et al., 2018b; for review see Dinniman et al., 2016; Asay-Davis et al., 2017). Their results for present day conditions, however, often disagree with available observations and vary widely between models (e.g., see Fig. 10 for estimates of basal mass loss from major ice shelves). Part of these discrepancies originate from boundary conditions and model design (e.g. Dinniman et al., 2015; Naughten et al., 2018b). The integrity of model dynamics, however,
35 is also questionable, since certain physical processes that have been identified as critical in regional studies, have not yet been included in large scale applications (Dinniman et al., 2016). One of these critical processes is ocean tides, which interact with ice shelves in several ways, most importantly through ice shelf basal melting (Padman et al., 2018). Regional studies have shown that tidal currents can heavily modulate local melt rates (e.g Makinson et al., 2011; Mueller et al., 2012, 2018), but, to our best knowledge, tides have not yet been included in Antarctic-wide ocean-ice shelf models. Further, large scale models are
40 typically run at coarse horizontal resolutions (10-20 km), which are not sufficient to resolve bathymetric troughs and eddies on the continental shelf (Dinniman et al., 2016). Both of these features, however, have been identified to transport heat from the deep ocean shoreward and not resolving them leads to underestimates of ice shelf melting in some regions (for the importance of troughs see Thoma et al., 2008; Assmann et al., 2013; for eddies see Stewart and Thompson, 2015; Stewart et al., 2018). Resolving tides and eddies is expensive, as they require a fine temporal and spatial discretisation, but including them in large
45 scale models is seen as a major step towards more accurate representations of the polar regions.

Model evaluation and efficient tuning is hindered by sparse in situ observations, both beneath ice shelves and on the continental shelf. Model parameters in regional studies are usually calibrated (e.g. Nakayama et al., 2017), but to approach similar efforts with large scale models, suitable Antarctic-wide observations need to be compiled first. Nevertheless, evaluation of selected quantities helps to identify large biases and evaluate model performance. For this purpose, previous studies have often
50 utilised ice shelf melt rates derived from satellite observations and models of firn processes (e.g. Schodlok et al., 2016), and selected Southern Ocean quantities from observations and reanalysis products (e.g. Naughten et al., 2018b). These measures, however, have limitations. For example, while satellite studies provide uncertainty bounds for melt rates averaged over ice shelves or ice flow lines (as in Rignot et al., 2013; Depoorter et al., 2013; Liu et al., 2015), the uncertainty of high resolution data is unknown. Further, ocean reanalysis products, such as the Southern Ocean State Estimate (SOSE; Mazloff et al., 2010),
55 assimilate most of the available data from elephant-seals, ships and Argo Floats, but observations on the Antarctic continental

shelf are sparse and the underlying ocean models do not account for ice shelf melting and, hence, the resulting freshwater release.

Here we describe the development and evaluation of a new circum-Antarctic ocean-ice shelf model that aims to overcome some of the shortcomings of previous studies. The Whole Antarctic Ocean Model (WAOM v1.0) includes tides and an eddy

60 resolving horizontal resolution of 2 km and, thus, includes all the model physics of state-of-the-art regional applications. Establishing an evaluation matrix and rigorous model tuning is out of the scope of this study, but we aim to convince the reader that WAOM is capable of simulating an equilibrated and realistic version of present day conditions by comparing model results against a selection of established estimates of Southern Ocean quantities and ice shelf melting for the chosen period of 2007.

The following section (Sect. 2) describes the model and experiments performed in this study. In Section 3, we evaluate

65 tidal accuracy, investigate resolution effects and compare model results against selected off-shelf hydrography from SOSE, as well as estimates of ice shelf-ocean interaction from regional studies and large scale satellite observations. This is followed by a discussion of WAOM's key strengths and limitations, as well as future development and research questions suitable for exploration with our model (Sect. 4). The last section (Sect. 5) summarises and concludes this study.

2   Model Description

70 ### 2.1   General Approach

The code that is underlying WAOM has been developed over a decade by our research group in Tasmania and established its integrity in the wider community in many regional and idealized applications (Galton-Fenzi et al., 2012; Cougnon et al., 2013; Gwyther et al., 2014, 2016). In this study we use our experience to upscale the code to a circum-Antarctic domain. WAOM v1.0 (Richter, 2020a) and the scripts used for pre- and post-processing (Richter, 2020b) are open source and can be downloaded

75 and developed on github.

2.2   ROMS and Ice-Ocean Thermodynamics

WAOM's backbone is the Regional Ocean Modeling System (ROMS v3.6). ROMS is a free-surface, terrain-following, primitive equations ocean model framework (Shchepetkin 2005) that allows treatment of advection and diffusion in the ocean in a multitude of ways and on different grid configurations. For WAOM we use a curvilinear coordinate grid (south polar pro-

80 jection) and solve, for example, horizontal and vertical tracer advection using the 4th-order Akima advection scheme, while closing turbulent vertical mixing with the scheme from Large et al. (1994) (see Tab. C1 and C2 for all activated options and key parameter choices, respectively).

For ice ocean-thermodynamics, we use the 3-equation melt parameterisation developed by Hellmer and Olbers (1989), refined by Holland and Jenkins (1999) and implemented into ROMS by Galton-Fenzi et al. (2012). The parameterisation accounts

85 for thermal and haline driving across the ice-ocean boundary layer, velocity dependent exchange coefficients following McPhee

(1987) and the case of molecular diffusion alone Gwyther et al. (2016). The exact equations used for ice-ocean interaction in WAOM are described in Gwyther et al. (2016).

2.3 Domain, Topography and Spatial Discretisation

The rectangular domain is shown in Figure 1 and covers all of the Antarctic ice shelf cavities and adjacent continental shelf
90 regions. Spatial discretisation in the vertical uses 31 terrain-following layers with enhanced resolution at top and bottom and results in top layer thicknesses under the ice varying from 0.5 m to 8.3 m (stretching function and parameters used in transformation equations shown at Tab. C2). In the horizontal we apply uniform grid spacing with resolutions of 10 km, 4 km and 2 km, which results in 52, 130 and 260 million computational cells, respectively. We note that the design of WAOM requires masking of about 36 % of the cells due to land area.

95   The ice draft and bottom topography south of 60 °S have been derived from Bedmap2 (Fretwell et al., 2013) and north of 60 °S (outside the Bedmap2 boundaries) have been taken from RTopo-2 (Schaffer et al., 2016). Calculating the horizontal pressure gradient at steep sloping topography in terrain-following coordinates is known to generate spurious currents and mixing (Mellor et al., 1994, 1998). ROMS is designed to minimise this issue by applying the splines density Jacobian method for the calculation of the pressure gradient force. Nevertheless smoothing of bathymetry and ice draft is recommended (e.g.
100 Sikirić et al., 2009), in particular considering the almost vertical cliff face at the ice shelf front (also discussed in Naughten et al., 2018b). Using the Mellor-Ezer-Oey algorithm (Mellor et al., 1994) we smooth the bathymetry and ice draft iteratively until a maximum slope factor $r = (h_i - h_{i+1})/(h_i + h_{i+1}) \leq 0.3$ is satisfied (h describes either water column thickness or sea floor depth). Further, for numerical stability, we artificially deepen the bathymetry in shallow ice shelf grounding zones to obey a minimum water column thickness of 20 m. While this step might impact local ice shelf ocean-interaction, it has been
105 shown not to affect ice shelf average melt rates and 20 m is considered one of the smallest modifications possible (Schnaase and Timmermann, 2019).

    Table 1 summarises the computational costs associated with running the model on the Australian National Computing Infrastructure (NCI) supercomputer Raijin. On the resulting grids with 10 km, 4 km and 2 km resolution the 3-D equations integrate stably with timesteps of, respectively, 900 s, 360 s and 180 s. This leads, for example, to a cost of 6,800 CPU hours
110 for 1 year of simulated period at 4 km resolution. We note that upscaling of the computational architecture for the highest resolution was obscured by the fact that the parallel input-output was not functional. Serial input-output puts the computational burden onto a single CPU, requiring us to choose a suboptimal architecture with few CPUs and large RAM per CPU. This issue should be addressed in future studies.

2.4 Forcing and Boundary Conditions

115 At the surface, we apply daily buoyancy fluxes derived from sea ice concentration observations (Tamura et al., 2011) and daily wind stress calculated from ERA-Interim 10-m winds and bulk flux formula (Dee et al., 2011). Prescribing surface buoyancy fluxes, rather than including a sea ice model, is likely to more accurately capture polynyas that form in the lee of fast ice and icebergs, and are critical to resolve accurate ice shelf melting in cold regimes (see Mode 2 melting described in Jacobs et al.,
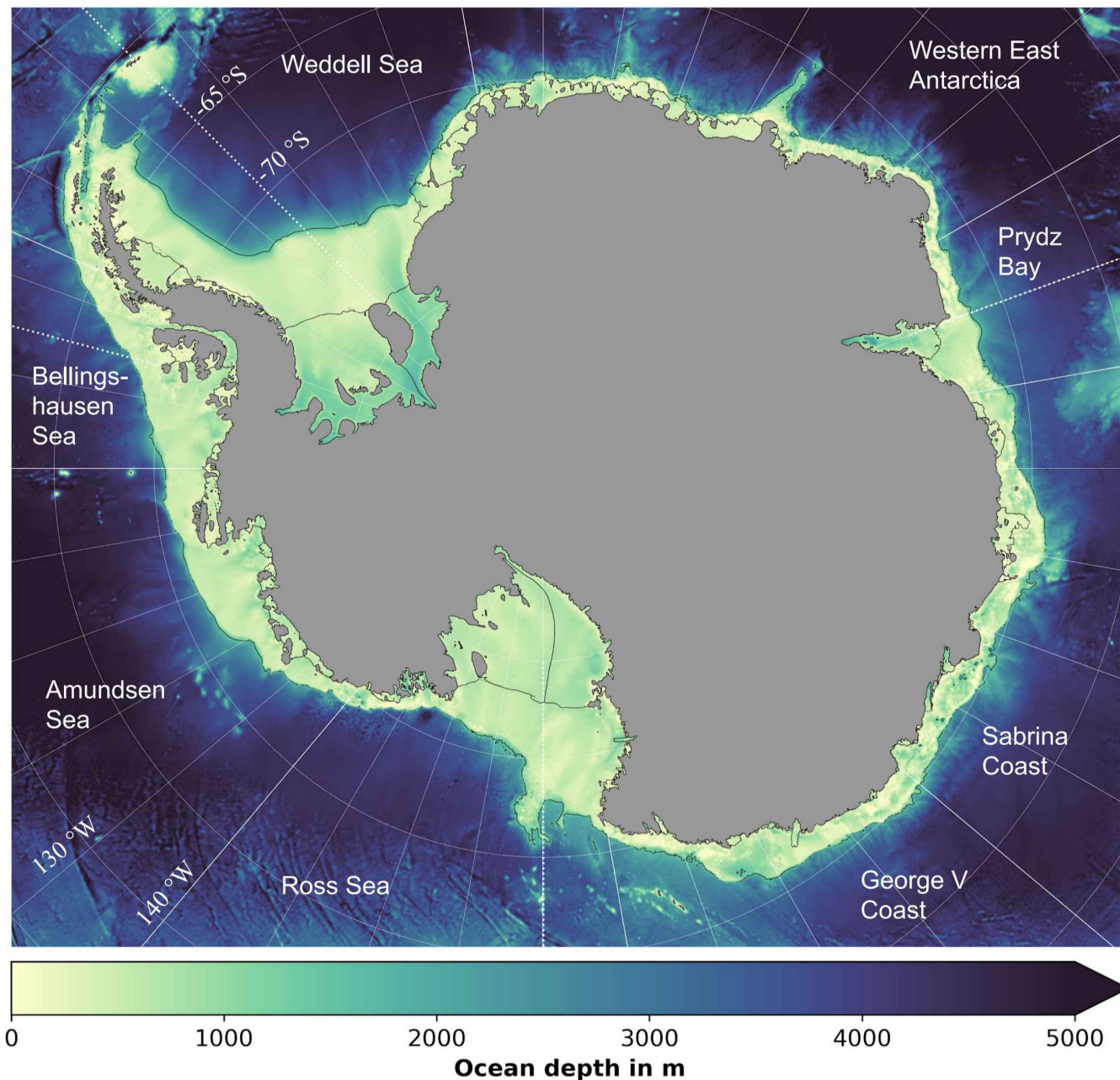
Figure 1. Model domain and bathymetry. Figure boundaries denote the model domain and colors show sea floor depth (also inside the sub-ice shelf cavities). Thin black lines are boundaries for the ice shelves and the continental shelf used in this study. Thin white lines are longitudes and latitudes. Labels denote ocean sectors, while bold white lines indicate their boundaries. Dotted white lines are longitude transects used in Figs. 7a to 7d.

Model Resolution	10 km	4 km	2 km
Period simulated	1 year	1 year	1 year
CPU hours	280 h	6,840 h	40,030 h
Architecture	Sandy Bridge	Sandy Bridge	Broadwell
Number of CPUs	256	2304	224
Memory	51 GB	2.9 TB	876 GB
Walltime	1 h	3 h	142 h
Storage for 1 3D field	40 MB	250 MB	1 GB

Table 1. Computational requirements at different resolutions. WAOM has been run on the supercomputer Raijin from the National Computing Infrastructure (NCI) in Australia. Sandy Bridge architecture stands for 2x8 core Intel Xeon E5-2670 2.6GHz with 32 GB RAM per node and Broadwell is 2x14 core Intel Xeon E5-2690v4 2.6GHz with 128 GB RAM per node. We needed to ensure a high RAM per CPU for the 2 km application as input-output was handled in serial.

1992). We tune the surface forcing by reducing positive heat flux into the ocean to half its original value, omit brine injection

120 when the ocean is warmer than the freezing point and relax surface temperatures towards freezing when they are being forced below freezing. Further, to avoid model drift, the surface ocean is relaxed over long timescales to the solution from SOSE (Mazloff et al., 2010), using a heat flux into the ocean of $40\,\mathrm{W\,m^{-2}\,{}^\circ C^{-1}}$ and a salinity relaxation timescale of one month. We do not account for the effect of sea ice on wind stress or frazil ice formation (as in, e.g. Galton-Fenzi et al., 2012).

Open boundary conditions are taken from the ECCO2 reanalysis (Menemenlis et al., 2008) and consists of monthly values

125 for sea surface height, barotropic and baroclinic velocities, and temperature and salinity. The model solution, however, mostly dictates the conditions at the boundary, as we nudge inflow and outflow with timescales of 1 day and 1 year, respectively. Initial ocean temperatures and salinities for January 2007 are also derived from ECCO2 and values under the ice shelves are extrapolated from the ice front. Thirteen major tidal constituents (M2, S2, N2, K2, K1, O1, P1, Q1, MF, MM, M4, MS4, MN4) are derived from the global tidal solution TPXO7.2 (Egbert and Erofeeva, 2002) and also introduced along the northern

130 boundaries of WAOM using sea surface height and barotropic currents.

2.5 Spin Up and Experiments

For this study we simulate the year 2007. Forcing with single year conditions captures daily to seasonal variability, while allowing us to run the model to quasi-equilibrium with our given supercomputing resources. At the time of development, all data products used to force the model covered the period from 2005 to 2011 and we found that sea ice buoyancy fluxes and

135 wind stress from the year 2007 are a non-anomalous representation of the period from 1992 to 2011.

To further save computational costs we perform most of the spin up at lower horizontal resolutions. This idea takes advantage of the fact that the temporal and spatial scales of ocean processes are correlated, that is the largest spatial features, such as the Weddell Sea gyre, also take the longest time to develop. Figure 2 visualizes our spin-up procedure. The 10 km version of

the model is integrated for 5 years, before the on shelf ocean reaches a quasi equilibrium and its solution is used to initialise

140   the 4 km run. Analogously, the 4 km run is stepped forward in time for 2 years before the final 2 km simulation is initiated and integrated for another year and three months. Interpolation of lower resolution solutions to the higher resolution grids is performed using a nearest neighbour method. This can result in artificially large pressure gradients between neighbouring cells, causing model instability. We address this issue by running the first day of each high resolution simulation with a reduced timestep. The ocean state after one day is then used to initiate the actual high resolution run. Diffusivity and viscosity

145   coefficients have been reduced in proportion to to grid refinement (see C2). The main results are taken from the final year of the 2 km run.
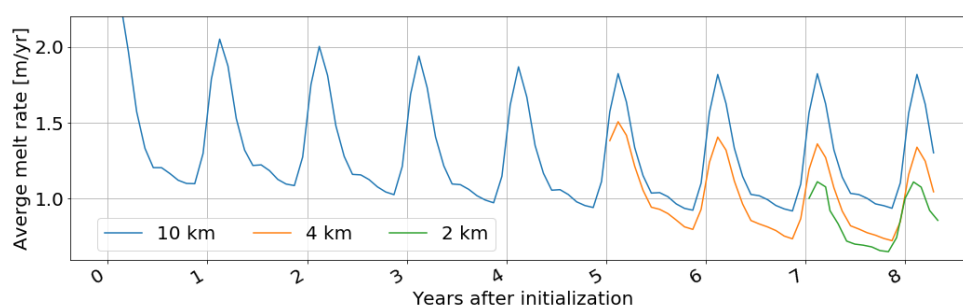
Figure 2. Spin up procedure. We spin up large scale processes at lower resolution and find that ice shelf average melting is a good diagnostic for the state of the continental shelf ocean. This way, the total spin up time for the final year of the 2 km-resolution solution is 7 years and 3 months. Model output is plotted as average of every month.

2.6   Analysis

To calculate basal mass loss from individual ice shelves we use ice shelf boundaries from the MEaSURES Antarctic boundaries dataset (Mouginot et al., 2016). This dataset reflects the 2007 state, while Bedmap2 ice thickness data is mostly based on laser

150   altimetry data from 1994 to 1995. Restricting the ice shelf area to the intersect of Bedmap2 and MEaSURES excludes parts of the ice shelf front in some regions and a narrow frame of thin ice along the open coastlines (see Fig. B1).

We use SOSE to evaluate the off-shelf ocean. As mentioned earlier, SOSE assimilates many observations from elephant-seals, ships and Argo floats in the Southern Ocean, making it very reliable where such observations exist (Mazloff et al., 2010). On the shelf, however, observations are sparse and the ocean dynamics used to integrate SOSE do not include ice shelf

155   interaction. Hence, we expect SOSE to have large biases close to the ice and we only use its solution for the off-shelf ocean to evaluate WAOM.

3 Results

3.1 Tides Evaluation

Following King and Padman (2005), we assess the accuracy of tides in the model by comparing tidal height signals against
69 Antarctic Tide Gauge (ATG) station data, including observations from tide gauges, gravimetric data and GPS records of
ice shelf surface elevation. For this we use 365 days of hourly sea surface elevation model output from the 10 km-horizontal
resolution simulation. Evaluating tides at higher resolution would have taken considerably more resources and we expect the
improvement of accuracy with finer grid spacing to be incremental. We interpolate the model data to the coordinates of each of
the 69 tide gauge stations using nearest neighbour interpolation. For the four major tidal constituents M2, S2, K1 and O1, we
recover amplitudes H and phases G from the sea surface height time series using classical tidal harmonic analysis (Pawlowicz
et al., 2002), and then calculate the complex amplitude $Z = H \cos G + i \sin G$ as a representation of the tidal energy. We
disregard stations for a certain constituent if no ATG data is available, the nearest ocean cell is further than 50 km (5 grid cells)
away or the tidal harmonic analysis fails to converge. The Antarctic-wide accuracy of complex amplitudes for each constituent
is assessed using root-mean-square (RMS) errors (defined as σ_x) as follows:

$$\sigma_x = \sqrt{\frac{1}{2N} \sum_{j=1}^{N} \left[Z_j^m - Z_j^o \right]^2}, \tag{1}$$

whereby m and o superscripts denote modelled and observed, respectively, and N is the number of stations. To get a single
measure for model bias in tidal energy, the combined RMS error is calculated as

$$\sigma_{comb} = \sqrt{\frac{1}{2N} \sum_{k=1}^{4} \sum_{j=1}^{N} \left[Z_j^m - Z_j^o \right]^2}, \tag{2}$$

where the differences are also summed over all four constituents k = [M2,S2,O1,K1].

The model has a combined RMS error of 27 cm, 17 % higher compared to an RMS error of 23 cm for state-of-the-art 2D
Antarctic tide models assessed in King and Padman (2005). Table 2 summarizes the outcomes of the tidal height accuracy
analysis, while Figure 3 shows complex amplitude differences for each of the four constituents at each tide gauge station. Most
of the bias comes from the semidiurnal constituents M2 and S2 and from sites at the grounding line deep under the large ice
shelves. In these shallow regions, semidiurnal tides reach maximum amplitudes of 3 metres (e.g. Griffiths and Peltier, 2008),
while bathymetry and ice draft are very uncertain. Tidal strength is sensitive to water column thickness and, thus, we attribute
most of the tidal bias in WAOM to uncertainties in the sub-ice shelf cavity geometry of Bedmap2. Also, some bias might
originate from the imposed 20 m minimum water column thickness in shallow regions (see Sect. 2.3).

	M2	S2	O1	K1
Number of ATG stations	101	94	87	79
RMSD amp in m	0.23	0.18	0.07	0.09
RMSD phase in deg	27.14	22.65	8.92	8.30
RMSD complex amp in m	0.20	0.15	0.06	0.07
Combined complex RMSD in m		0.27		

Table 2. Summary of tidal height comparison against Antarctic Tide Gauge Records using Root-Mean-Square-Differences (RMSD).
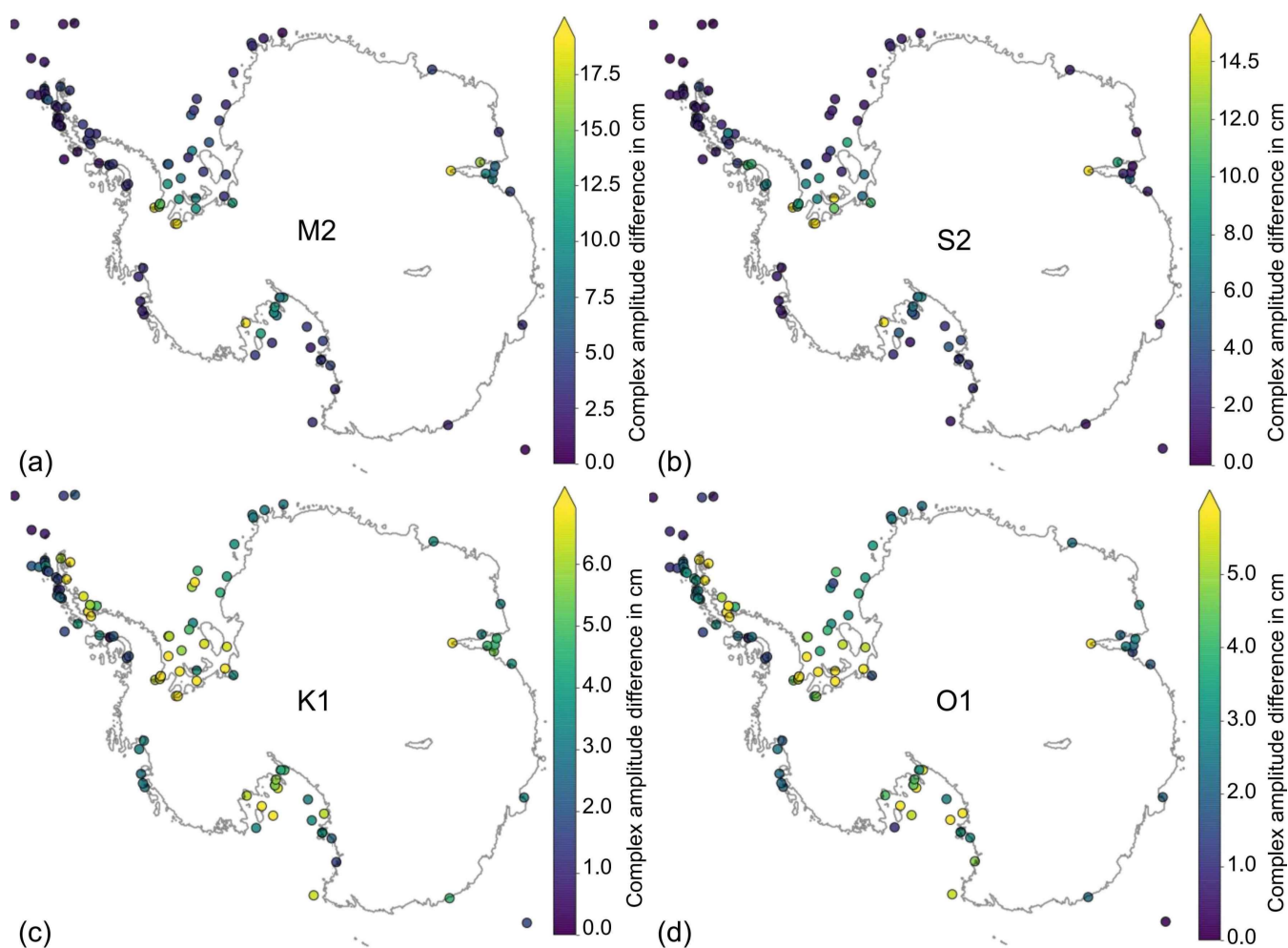
Figure 3. Spatial distributions of tidal height accuracy. Complex amplitude differences between the model solution and Antarctic Tide Gauge records are shown for the major tidal constituents (a) M2, (b) S2, (c) K1 and (d) O1. The largest biases occur at the deep grounding lines of the large ice shelves, where the water column thickness is uncertain.

3.2 Resolution Effects

The model solution of the continental shelf ocean converges with increasing resolution. We assess the impact of horizontal
185   resolution on the continental shelf ocean by analysing changes in annual mean ocean temperature and average ice shelf melting.
To ensure consistency, we compare the 2 km result against lower resolution solutions with equivalent overall simulation time,
that is 365 days after 7 years and three months (the overlap in Fig. 2). The results of the grid convergence study are shown
in Figure 4. We find that ocean temperatures as well as melt rates converge when increasing the grid resolution first from
10 km to 4 km (equivalent 250 %) and then to 2 km (equivalent 500 %). Grid convergence confirms that we start resolving
190   the processes most critical to our problem. The model solution, however, has not yet reached asymptotic behaviour, motivating
further refinement.
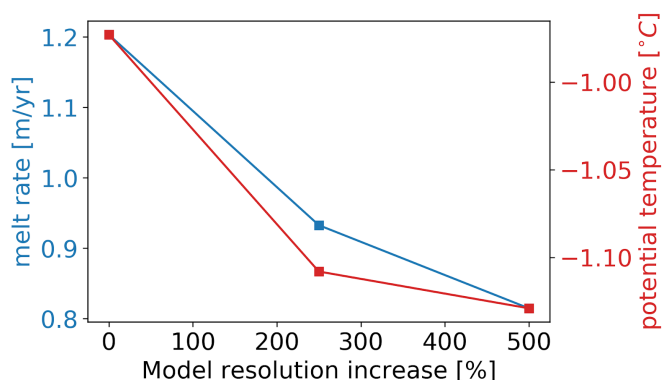
Figure 4. Grid convergence. Annual means of average melt rate and continental shelf potential temperature resolved at the different horizontal
resolutions: 10 km (0 % increase), 4 km (250 % increase) and 2 km (500 % increase). Continental shelf temperatures have been calculated
for depths shallower than 1500 m and including the ice shelf cavities (see Fig. 1). Continental shelf processes converge when grid spacing is
refined.

When increasing the grid resolution from 10 km to 4 km, the shelf ocean cools at many places, most likely due to better
resolved tidal processes. We find that resolution-induced changes in depth averaged temperature are governed by changes in
the bottom sigma layer (not shown). Figure 5 shows how bottom sigma layer temperatures change with increasing resolution.
195   The ocean cools at many places when refining the horizontal grid spacing from 10 km to 4 km (Fig. 5a). Differences exceed
1 °C in the eastern Bellingshausen Sea and in the eastern Ross Sea, and are on the order of 0.25 °C in the Amundsen Sea and
around the East Antarctic coastline. We attribute most of these changes to better resolved tidal processes, based on additional
sensitivity experiments that remove the tides (not shown). For example, activating tides in the model at 4 km resolution also
leads to warm water intrusions that extend under the north-western part of the Ronne Ice Shelf and ocean temperature changes
200   that resemble a dipole pattern in the eastern Ross Sea. Also, in both cases, effects are well constrained by the continental shelf

break, where tides start to weaken with increasing water column thickness. Finally, the overall reduction in continental shelf temperature has a similar magnitude in both experiments.

In contrast, increasing the resolution further (from 4 km to 2 km, see Fig. 5b) leads to a warming of the Amundsen-Bellingshausen Seas continental shelf. Even though the shelf temperature of the total domain still decreases slightly at the
205 second resolution step, the Amundsen-Bellingshausen Seas is warming. As mentioned earlier, this phenomenon is often associated with shoreward heat transport by eddies that need a grid spacing on the order of 1 km to be resolved by ocean models (Dinniman et al., 2016; Mack et al., 2019). The cooling north of Nickerson, Sulzberg and Swinburne Ice Shelves might be a consequence of this warming, as the continental shelf current drives melt water from the Amundsen-Bellingshausen Seas mostly westward (Nakayama et al., 2017).

3.3 Off Shelf Hydrography

To assess the broad-scale hydrography simulated in WAOM, we compare results against SOSE (Mazloff et al., 2010), a high quality ocean reanalysis product (See Section 2.6). Figure 6 presents the temperature-salinity distribution for WAOM and SOSE. At depth WAOM agrees well with SOSE in many aspects. In both models we identify the presence of Circumpolar Deep Water (CDW), Modified Circumpolar Deep Water (MCDW), Low-Salinity Shelf Water (LSSW), Antarctic Bottom Water
215 (AABW), Weddell Sea Bottom Water (WSBW), and Ross Sea Bottom Water (RSBW). We note that High Salinity Shelf Water (HSSW) is poorly represented in both models (e.g. see Nicholls et al., 2009, their Fig. 3, for observed HSSW properties in the Weddell Sea), which is likely related to the representation of sea ice and resulting surface fluxes. Below 2000 m depth, WAOM's RSBW and WSBW are up to 0.5 psu saltier than suggested by SOSE. This discrepancy might in part originate from WAOM's boundary conditions, as ECCO2's bottom water features salinities of up to 34.7 psu (slightly more than SOSE; not shown).
220 Stronger water mass transformation in WAOM compared to SOSE, however, might also play a role, as WAOM's WSBW is in part saltier than 34.8 psu and this can not be explained with boundary conditions alone. An unambiguous attribution would require further investigations beyond the scope of this study.

At shallow depths, however, the models disagree. Antarctic Surface Water (AASW) tends to be several degrees warmer in WAOM compared to SOSE, where the surface is often close to freezing. As the deep and often salty ocean mixes with these
225 surface waters, different tails are shaped in T-S space. While WAOM's surface water is often warmer than the ocean at depth, temperatures and salinities of SOSE's upper ocean mostly resemble freezing conditions. Which of the models is more accurate close to the surface and what is causing the differences is not clear. Figure 8 shows the temperature-salinity distribution for WAOM on the continental shelf and separated by sector. These distributions show that the warm surface waters in WAOM are mostly restricted to the off-shelf ocean and likely driven only by regional phenomena in the Bellingshausen Seas.
230 In contrast to SOSE, WAOM is capable of resolving Ice Shelf Water (ISW). ISW is produced by ice-ocean interaction inside the ice shelf cavities and often forms characteristic linear signatures in T-S space (Gade lines, see Gade, 1979). The z-like signature of ISW in the Ross Sea is likely caused by continued mixing of ISW from one ice shelf inside the cavity of another ice shelf downstream and this further supports the presence of ice shelf teleconnections.
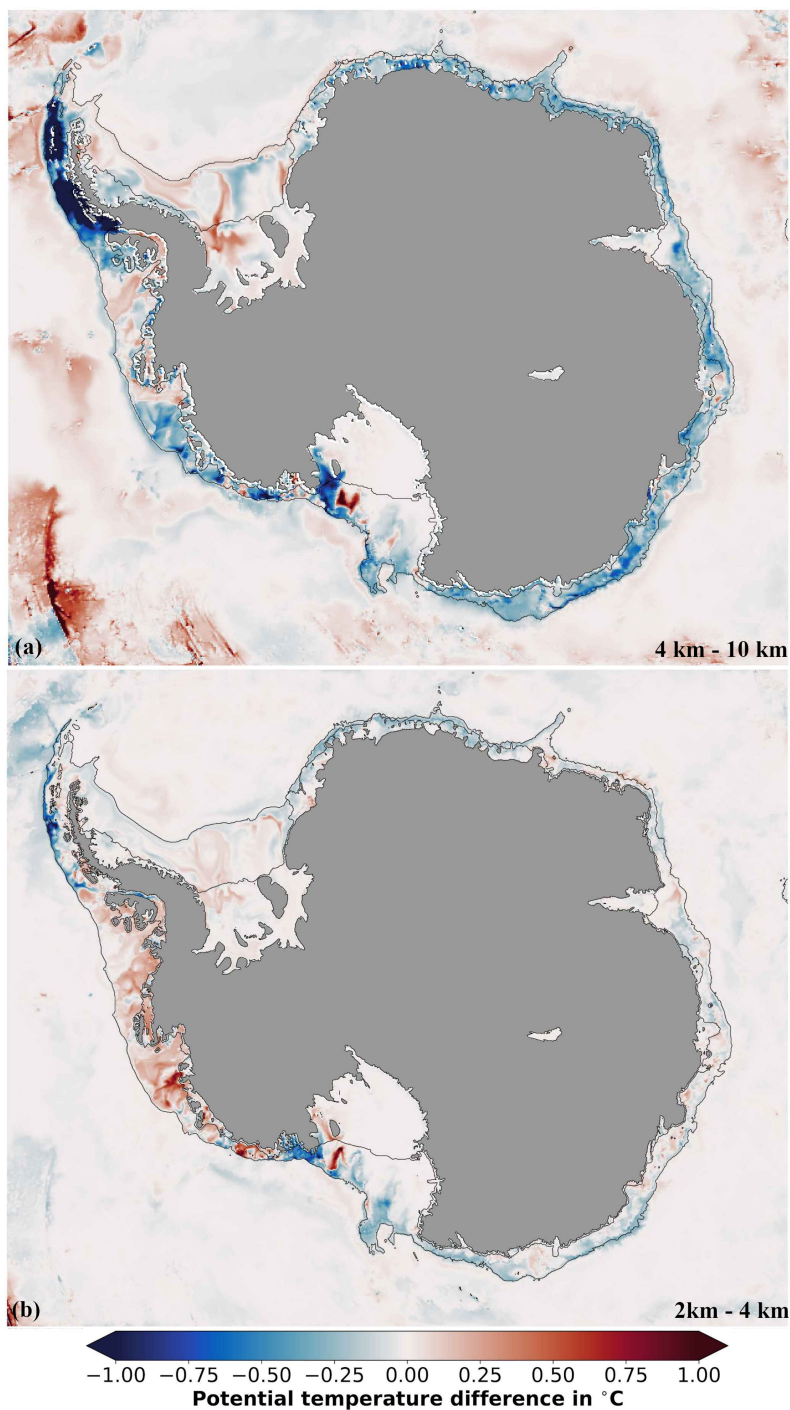
Figure 5. The effect of model resolution on bottom layer temperature. Change in annual average bottom sigma-layer potential temperature when increasing the horizontal model resolution from (a) 10 km to 4 km and (b) 4 km to 2 km. Black contour lines indicate the 1500 m isobath and ice shelf fronts.
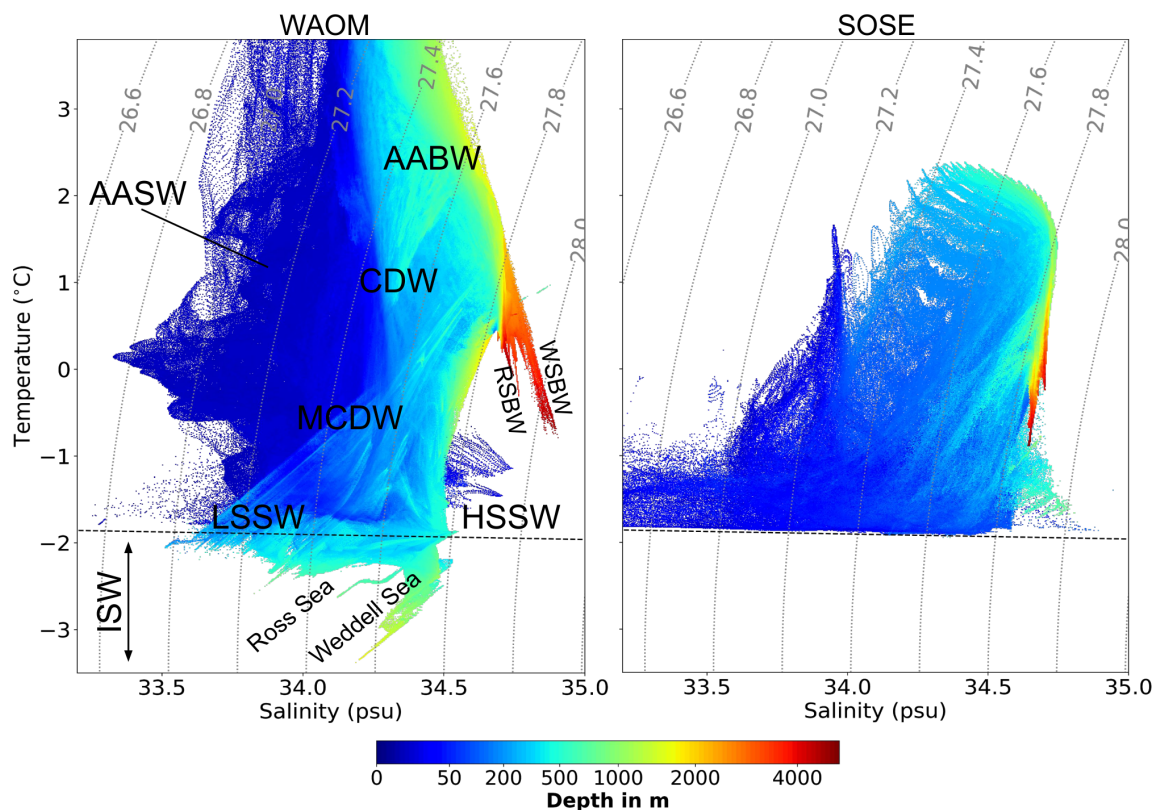
Figure 6. Water masses resolved by WAOM and SOSE. Potential temperature-salinity-depth distribution of the water masses apparent south of 65 °S in (a) WAOM and (b) SOSE. Each grid cell in either model has been sorted into 1000x1000 temperature and salinity bins and the depth shown for each bin is the volume-weighted average of all the grid cells in this bin. The dashed black lines show the freezing point at the surface and the dotted grey lines are potential density anomaly contours (in $\mathrm{km\,m}^{-3} - 1000$; referenced to the surface). Labels in (a) indicate the water masses Antarctic Bottom Water (AABW), Weddell Sea Bottom Water (WSBW), Ross Sea Bottom Water (RSBW), Circumpolar Deep Water (CDW), Modified Circumpolar Deep Water (MCDW), Low-Salinity Shelf Water (LSSW), High-Salinity Shelf Water (HSSW), Antarctic Surface Water (AASW) and Ice Shelf Water (ISW). Remaining labels indicate specific regions from where some water masses originate (also see Fig. 8).

The stratification of WAOM agrees well with SOSE for the off-shelf ocean and, as expected, diverges towards the ice

235 shelves. Figures 7a to 7d show longitudinal transects of temperature and salinity of both models. In the open ocean away from the continental shelf break, the solutions agree and this supports realistic boundary constraints and mixing processes in WAOM. Towards the shelf break and on the continental shelf WAOM resolves substantially colder and fresher waters compared to SOSE, which we interpret as the result of melt water from the ice shelf cavities.

WAOM also often shows stronger vertical mixing close towards the continental shelf, possibly caused by surface forcing,

240 tides or pressure gradient errors. The ocean close to the continental shelf is often well mixed in WAOM, but remains relatively stratified in SOSE (as, e.g., can be seen in Prydz Bay transect, Fig. 7d) and this could have various reasons. First, brine rejection in sea ice polynyas is known to cause deep mixing of the entire water column (e.g. Silvano et al., 2018). While WAOM and SOSE use the same mixed layer parameterisation (KPP), different surface forcing and melt water in WAOM might change the sensitivity to deep convection. Second, SOSE does not include tides. Tidal currents are known to contribute to ocean mixing and

245 tidal strength amplifies towards shallower waters (e.g. Padman et al., 2009). Finally, spurious currents from pressure gradient errors at steep sloping topography in sigma-coordinate ocean models might also contribute to more mixing in WAOM (Mellor et al., 1994, 1998). This argument is supported by the fact that WAOM produces enhanced mixing also in the vicinity of deep ocean ridges, e.g., in the Ross Sea (Fig. 7b).

3.4 On Shelf Hydrography

250 Observations on the continental shelf are sparse and cover only short periods of time, which often do not coincide with our simulation. Thus, we do not expect model results to closely match available measurements. Rather, in the following section, we showcase that the model qualitatively captures many of the known, critical features of the onshelf hydrography around Antarctica.

WAOM resolves the important water masses in the Weddell Sea, including Warm Deep Water (WDW) and large amounts of

255 ISW (as shown in Fig. 8; see Nicholls et al., 2009, their Fig. 3). Figure 9a shows a temperature-salinity transect in front of the Filchner Ice Shelf at 35 °W. This transect reveals that ISW resides at the bottom of the Filchner trough while warmer waters at mid depth resemble characteristics of Modified Weddell Deep Water or Eastern Shelf Water (also shown in Nicholls et al., 2009, their Fig. 7).

In contrast, deep waters in the Amundsen Sea sector feature some of the highest temperatures of the entire Antarctic conti-

260 nental shelf (see Fig. 8). Figure 9b shows the temperature and salinity distributions along 106 °W, indicating that these CDW intrusions are overlaid by colder Winter Water and only held stable by a large gradient in salinity (in agreement with, e.g. Jacobs et al., 2011).

Figure 9c shows a temperature-salinity transect on the continental shelf of Prydz Bay along 72 °E. Inside the Amery Ice Shelf cavity HSSW and ISW can be seen at the bottom and top of the water column, respectively. Further, we detect Dense

265 Shelf Water with salinities of more than 34.5 psu at depth greater than 500 m (Fig. 8, described by, e.g. Williams et al., 2016). CDW is held back from entering the continental shelf in this region by the Antarctic Slope Front (in agreement with, e.g. Guo et al., 2019, their Fig. 2).
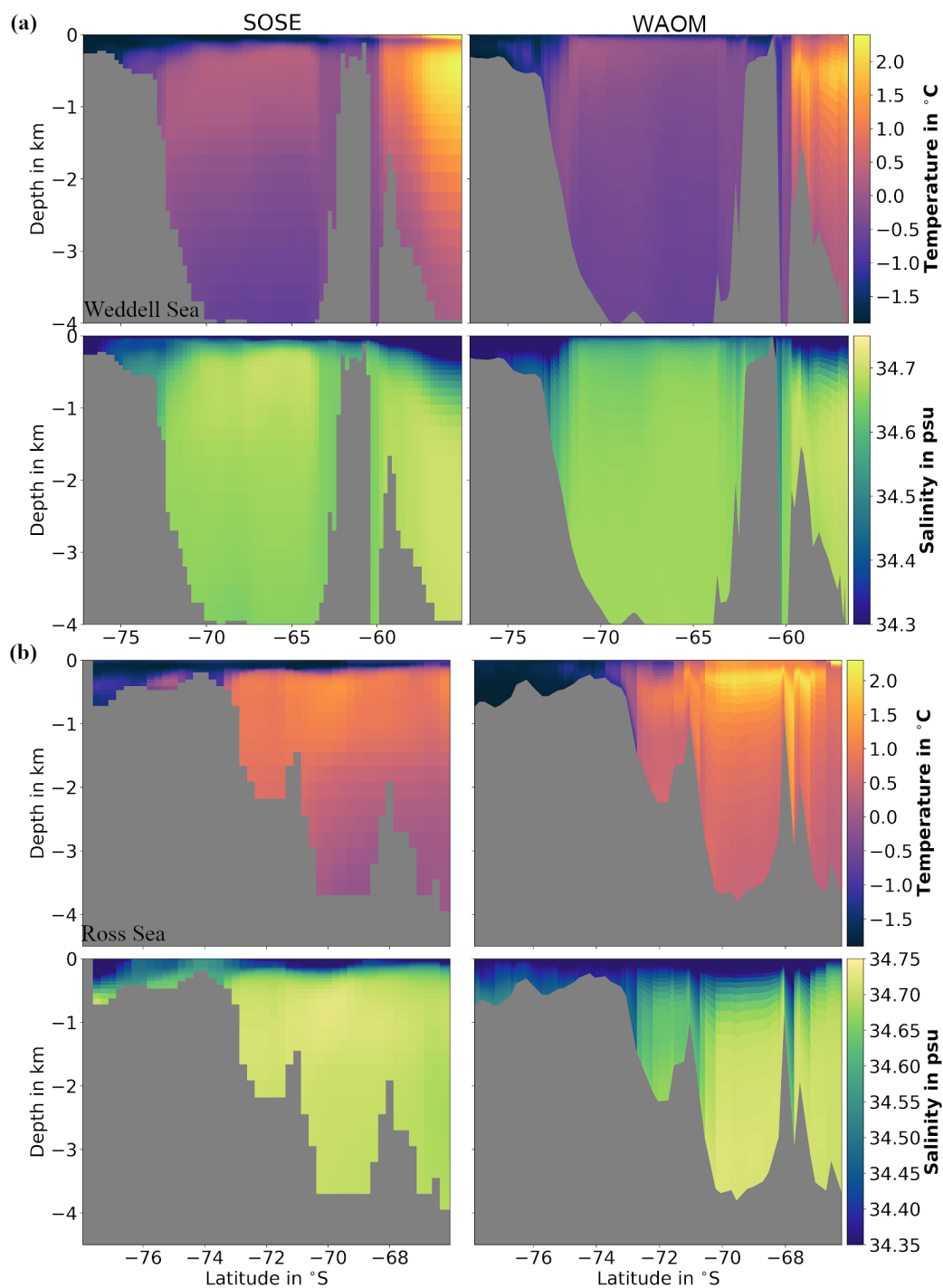
Figure 7. Temperature-Salinity distribution in (a) the Weddell Sea along 45 °W, (b) Ross Sea along 180 °W, (c) Bellingshausen Sea along 75 °W and (d) Prydz Bay along 70 °E. Transect locations are shown in Figure 1.
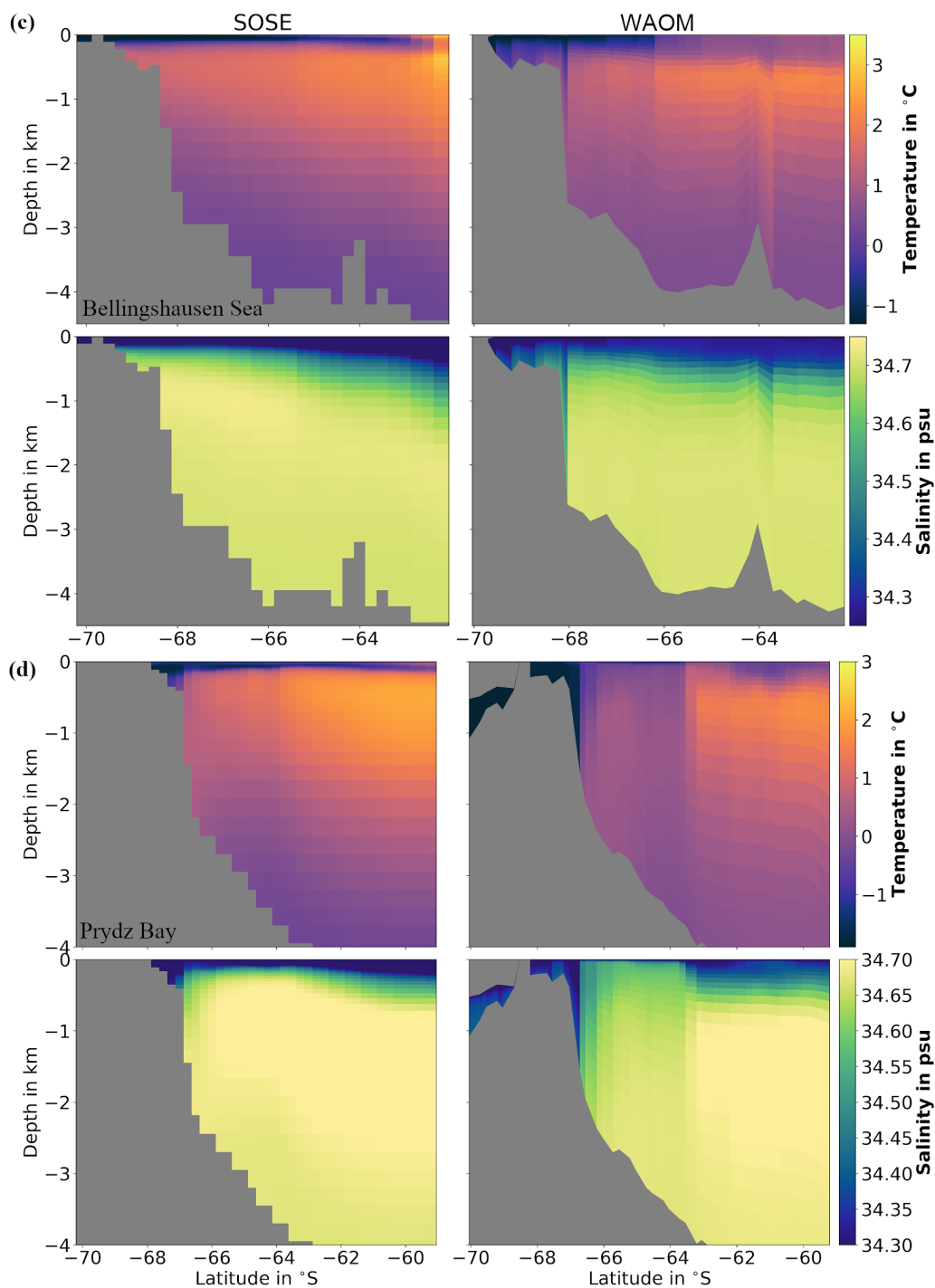
Figure 7. Temperature-Salinity distribution in (a) the Weddell Sea along 45 °W, (b) Ross Sea along 180 °W, (c) Bellingshausen Sea along 75 °W and (d) Prydz Bay along 70 °E. Transect locations are shown in Figure 1. (cont.)
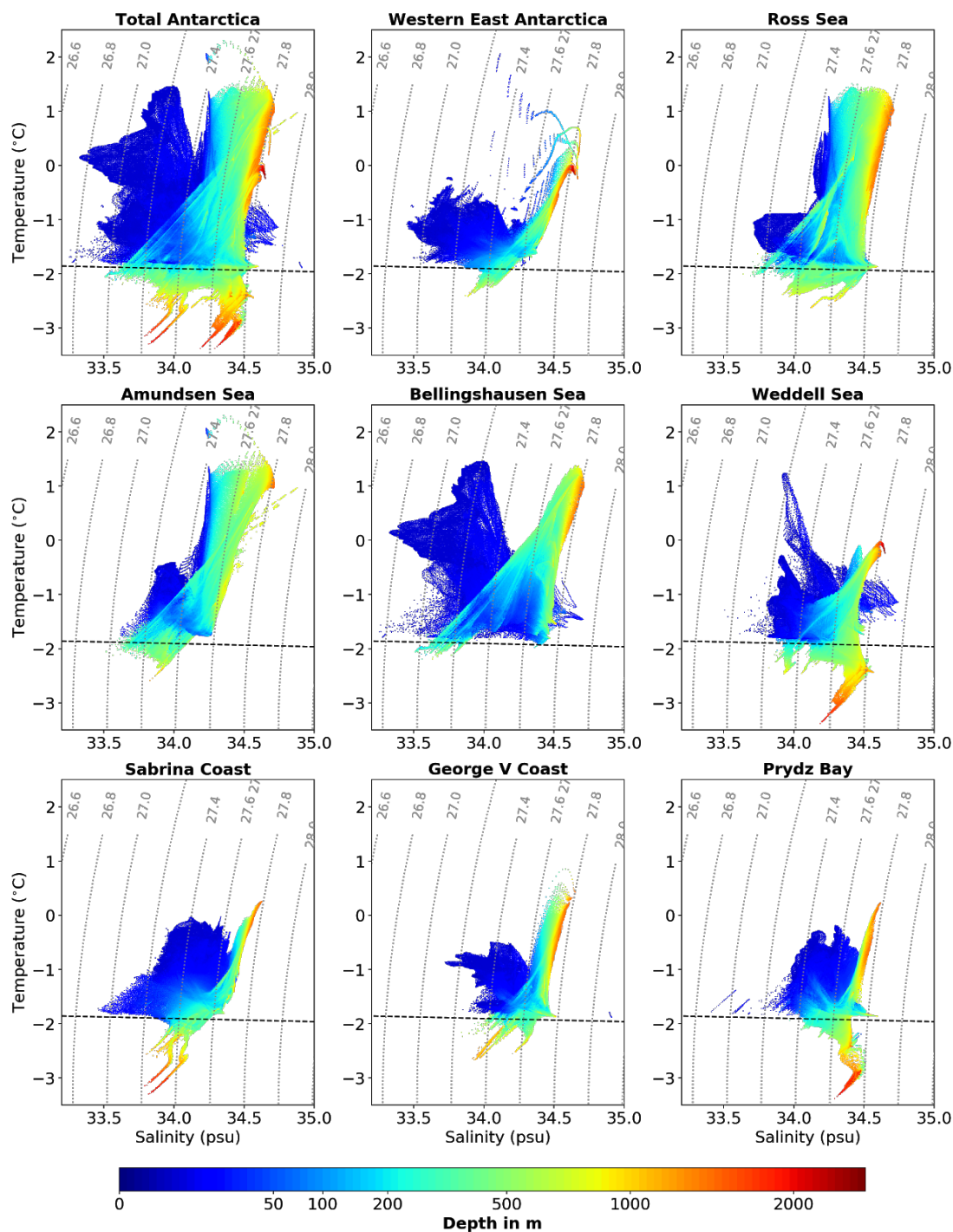
Figure 8. Water masses on the continental shelf for individual sectors. Same as Fig. 6a, but only for the continental shelf ocean and separated into individual sectors. The sub-ice shelf ocean is included and the continental shelf is defined using the 1500 m isobath (shown together with the sector boundaries in Fig. 1).
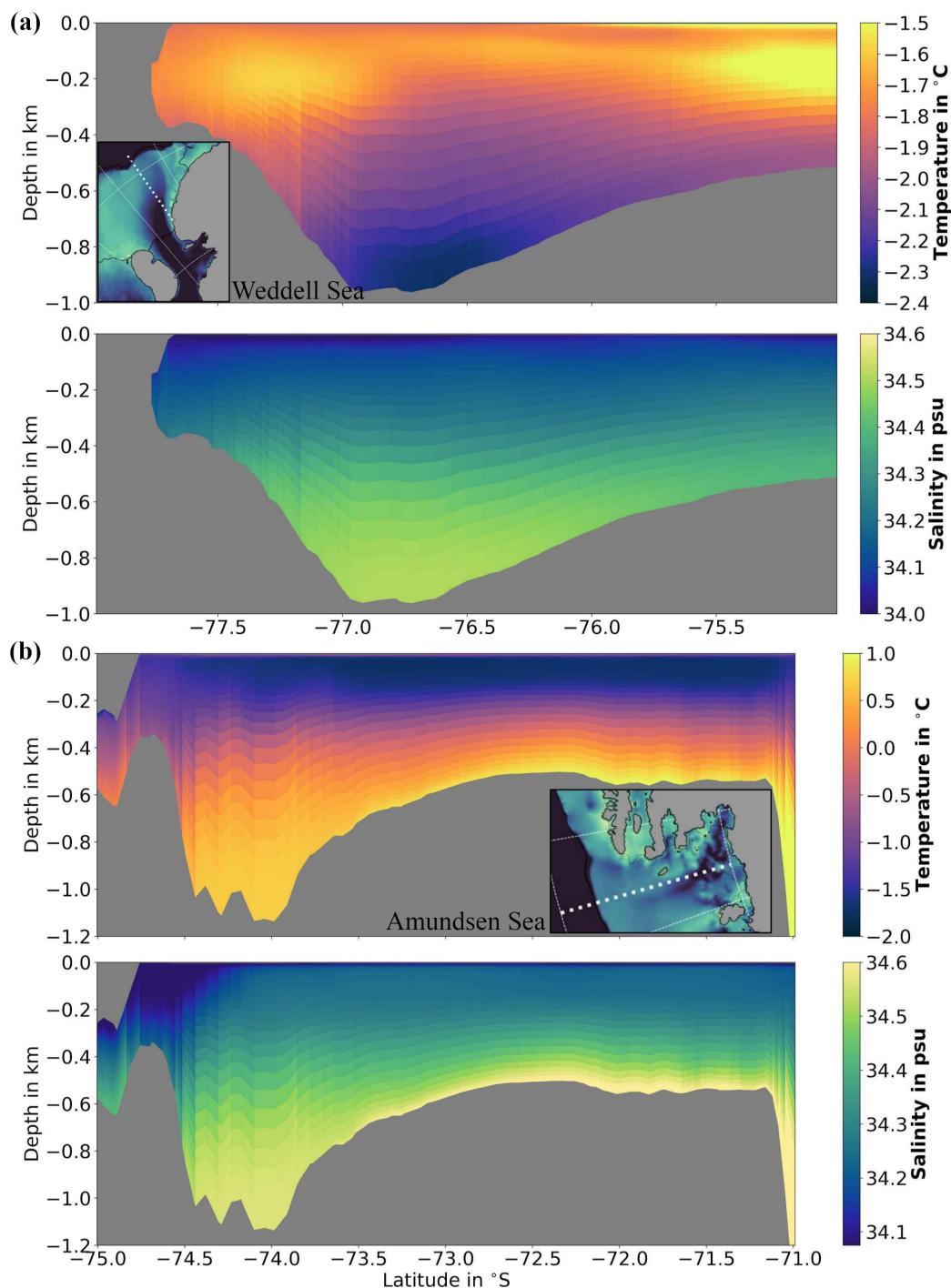
Figure 9. Temperature-Salinity distribution on (a) the Weddell Sea continental shelf at 35 °W, (b) the Amundsen Sea at 106 °W, (c) the Prydz Bay at 72 °E and (d) the Sabrina Coast at 120 °E. Inlets show the transect locations.
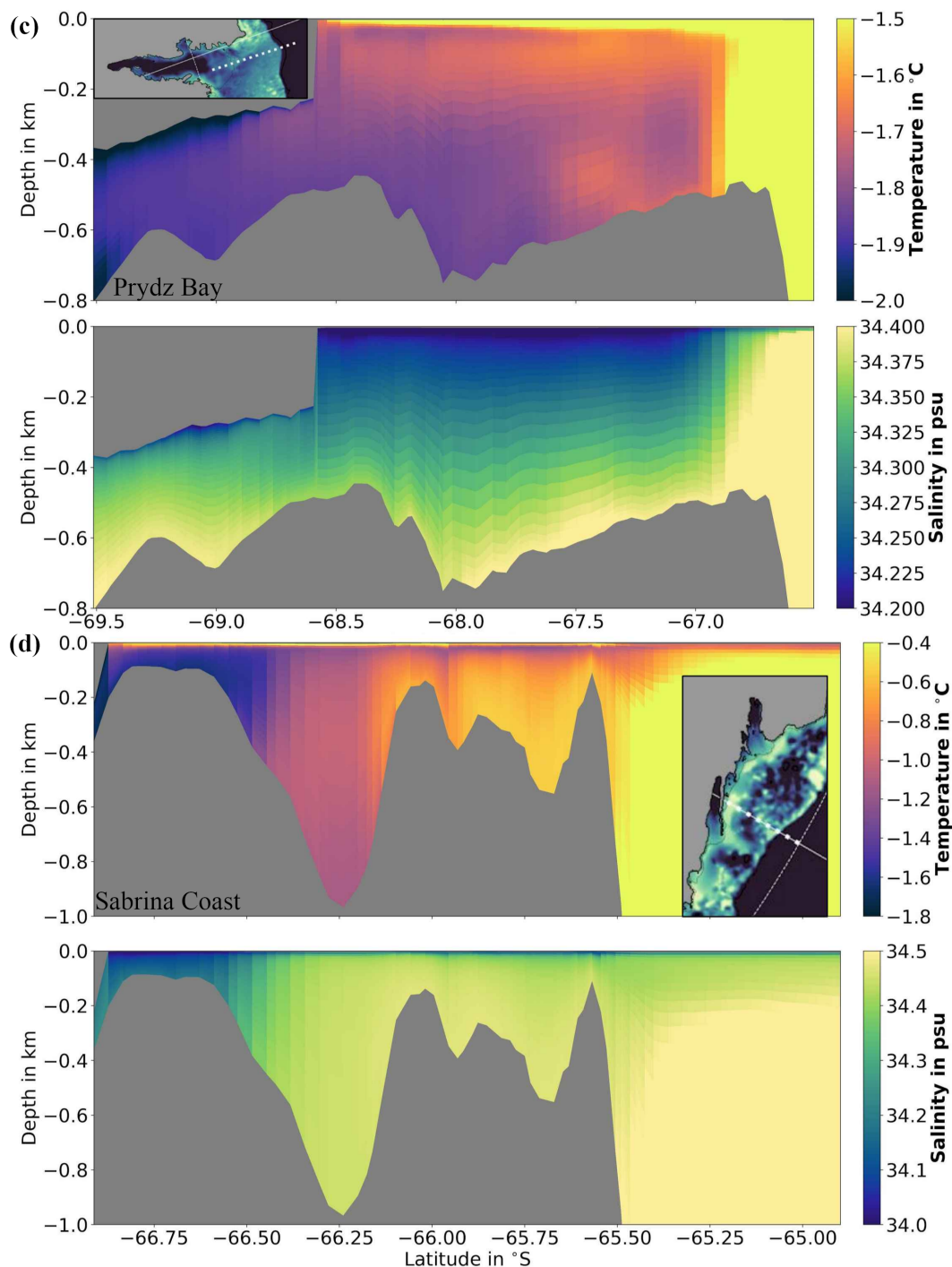
Figure 9. Temperature-Salinity distribution on (a) the Weddell Sea continental shelf at 35 °W, (b) the Amundsen Sea at 106 °W, (c) the Prydz Bay at 72 °E and (d) the Sabrina Coast at 120 °E. Inlets show the transect locations. (cont.)

Along the Sabrina and George V coasts, however, some MCDW crosses the continental shelf break, e.g. in front of the Totten Ice Shelf. This is demonstrated by the temperature-salinity distribution along 120 °E in Figure 9d. Once on the shelf MCDW competes with the lighter WW which occupies most parts of the shelf ocean close to the coast (in agreement with, e.g. Silvano et al., 2017, their Fig. 2 and 3).

AASW with temperatures well above freezing can be seen in all transects (Fig. 9a to 9d). We identify advection of these surface waters into the outer cavities of the Amery ice shelf (see Fig. 9c) and the Totten ice shelf (see Fig. 9d; in agreement with Silvano et al., 2017, their Fig. 2).

3.5 Ice Shelf Melting

Estimates of ice shelf basal mass loss generally agree with satellite observations in many regions. Figure 10 compares mass loss estimates for major ice shelves and Antarctica in total from this study against estimates from satellite observations and other ocean models (see Tab. A1 for underlying data). Using all ice in the model (according to Bedmap2, see Section 2.6), we calculate a total mass loss of 1209 Gt/yr (equivalent to an average melt rate of 0.82 m/yr). This is only 4 % below the range of estimates based on remote sensing data and models of surface processes (1263 Gt/yr to 1737 Gt/yr; Rignot et al., 2013; Depoorter et al., 2013; Liu et al., 2015). Regionally, the model and data show larger differences for some ice shelves (Pine Island, Getz, combined Brunt and Riiser-Larsen, Shackleton, combined Totten and Moscow University), but are in agreement or close to others (George VI, Abbot, combined Fimbulisen and Jelbart, Filchner-Ronne, Larsen C, Ross, Amery). In most regions of disagreement (Pine Island, Getz, Shackleton, combined Totten and Moscow University), satellite estimates suggest higher melting consistent with results from regional studies (e.g. Gwyther et al., 2014, for Totten and Moscow University Ice Shelves; Dutrieux et al., 2013, and Shean et al., 2018, for Pine Island Ice Shelf; Jacobs et al., 2013, for Getz Ice Shelf).

Melting and refreezing at high resolution shows that WAOM resolves many of the key features known from observations. Figure 11 presents ice shelf basal melt rates and bottom layer temperature around Antarctica from this study. In cold regimes, for example, HSSW often drives strong melting along deep grounding lines followed by refreezing along western outflows (defined as Mode 1 melting by Jacobs et al., 1992). WAOM's melt rates resemble this pattern at many places under the large cold water ice shelves in agreement with regional studies (e.g. under the Filchner-Ronne Ice Shelf in agreement with Holland et al., 2007; under the Larsen C Ice Shelf in agreement with Holland et al., 2009; under the Amery Ice Shelf in agreement with Galton-Fenzi et al., 2012).

It is further known that ice-ocean interaction in the Amundsen-Bellingshausen Seas is governed by intrusions of warm CDW that drive strong melting at all depths (Mode 2 melting; see, e.g. Pritchard et al., 2012; Rignot et al., 2013). WAOM resolves this mode of melting for most ice shelves in this region and features bottom layer temperatures comparable to that observed (often warmer than 1 °C; see, e.g. Schmidtko et al., 2014, their Fig. 1A; Pritchard et al., 2012, their Fig. 2).

WAOM also resolves other features in cold water regions that agree with observations. For example, the model indicates enhanced melting in the northwestern part of Ronne Ice Shelf, while predicting refreezing north of Henry Ice Rise and east of Berkner Island. All of these features are also reported by Joughin and Padman (2003) and Rignot et al. (2013), even though the magnitude and extent of marine ice accretion is generally lower in the model. Further, the model predicts elevated melt
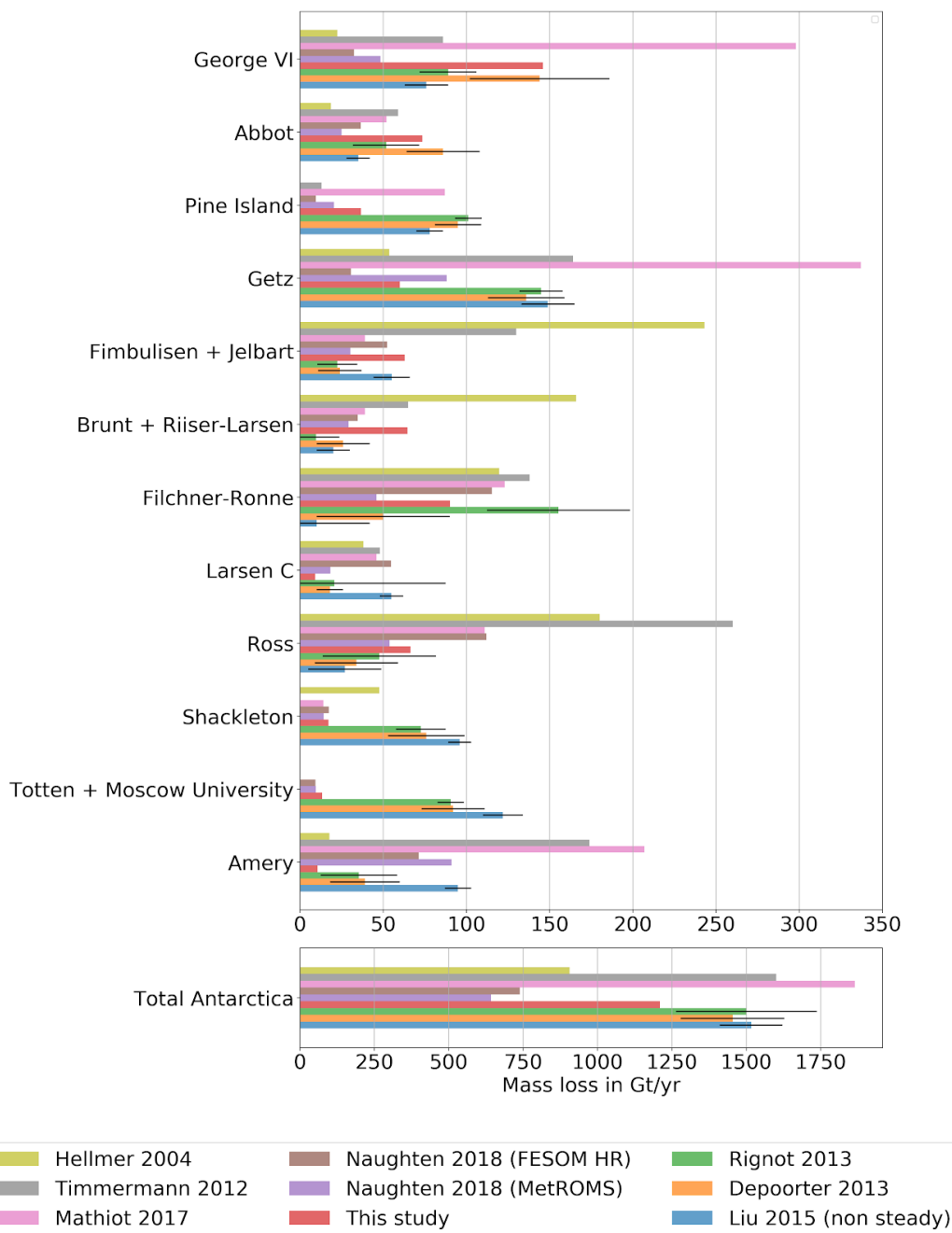
Figure 10. Ice shelf basal mass loss from models and satellite observations (equiv. Tab. A1). Estimates of ice shelf basal mass loss for total Antarctica and major ice shelves individually derived from previous ocean-models (Hellmer, 2004; Timmermann et al., 2012; Mathiot et al., 2017; Naughten et al., 2018b), this study and methods combining satellite data with models of surface processes (Rignot et al., 2013; Depoorter et al., 2013; Liu et al., 2015). Among the satellite studies, only Liu et al. (2015) avoids the assumption of a steady state calving front when inferring basal conditions (see Liu et al., 2015, for implications).
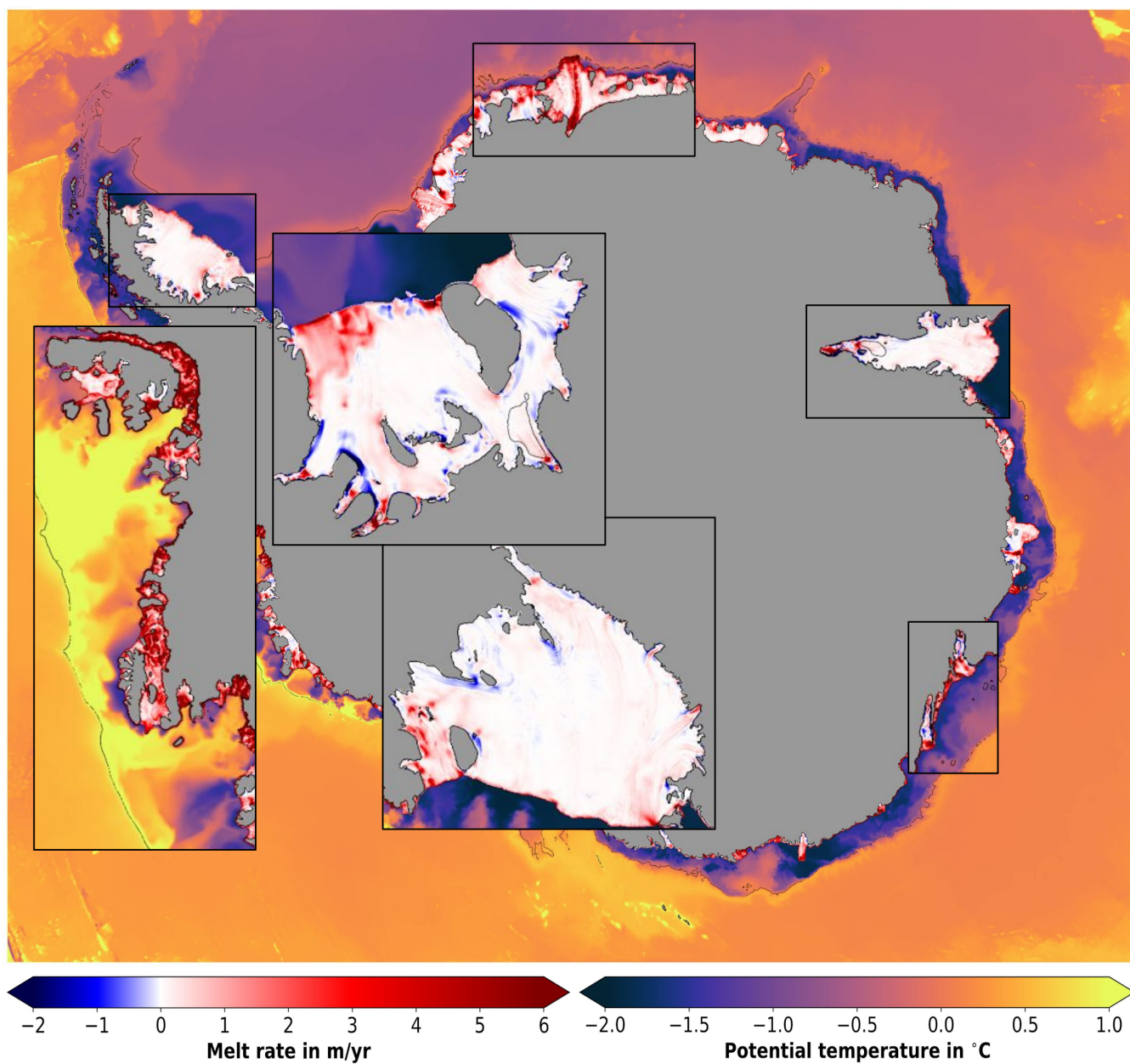
Figure 11. Ice shelf melting and bottom layer temperatures. Annual ice shelf basal melt rate is shown where ice shelves are present (negative is refreezing, note the shifted colorbar). Colors seaward of ice shelves show the annual average bottom sigma layer potential temperature. Thin black lines represent the 1500 m isobath.

rates along the deep keel of the Fimbul Ice Shelf and this has also been reported by a well constrained regional simulation by Hattermann et al. (2014).

The final melting mode (Mode 3) describes elevated melt rates close to the ice front and WAOM suggests that this melting
305 is apparent everywhere. Jacobs et al. (1992) hypothesise that intrusions of warm surface waters cause strong melting at the frontal zone of ice shelves (often defined as outermost 50 km) at most places around Antarctica. In situ observations have confirmed Mode 3 melting for parts of the Ross, McMurdow and Fimbul Ice Shelf (e.g. Hattermann et al., 2012; Stern et al., 2013; Stewart et al., 2019) and WAOM suggests elevated melt rates in all these regions, with melt rate magnitudes comparable to the observations: about 3 m/yr at the Ross ice shelf front (see Horgan et al., 2011; Stewart et al., 2019) and about 1 m/yr
310 at Windless Bight (see Stern et al., 2013). The simulation results further suggest ice shelf front melting is not limited to these regions, but rather is a widespread feature.

4 Discussion

Compared to other models, WAOM includes an eddy resolving resolution, tides and accurate polynyas, a first for a circum-Antarctic ice-ocean simulation. These features are critical for resolving ocean-ice shelf interactions accurately and, thus, we
315 consider ice shelf melting and the causal oceanic mechanisms at improved resolution as WAOM's most valuable contribution to ice shelf-ocean research. These melt rates are fully independent from satellite based approaches and will provide new, quantitative insights into the driving mechanisms of ice shelf melting in a pan-Antarctic context. Further, idealized studies have started to explore the average behaviour of the ice shelf cavity system, including its response to a warming ocean (e.g. Holland et al., 2008; Little et al., 2009; Gwyther et al., 2016; Holland, 2017). WAOM provides 176 realistic ice shelf cavities
320 with a single simulation spanning the entire range of present day geometries and ocean conditions. Exploring relations in the average quantities between these systems might help to extrapolate the overall future response of ice shelf melting around Antarctica. Finally, ocean-models are well suited for perturbation experiments and, in the case of WAOM, these can be used to study ocean-ice processes in more detail, for example, the impact of tides or ice shelf teleconnections.

Against expectations, coarsening the model resolution results in an overall warming of the continental shelf ocean and we
325 attribute this to less accurate resolved tidal processes. Previous studies without tides generally suggest a warming trend of the continental shelf when increasing the resolution from tens of kilometres to kilometres (e.g. Dinniman et al., 2015; Naughten et al., 2018b). This behaviour has been attributed to better resolved bathymetric features, such as troughs, and eddies that act to increase heat transport onto the shelf (Nakayama et al., 2014; Stewart and Thompson, 2015). The results presented here support the importance of shoreward heat flux by eddies and bathymetry in some regions, e.g., the Amundsen-Bellingshausen
330 Seas. The overall picture, however, is dominated by different processes. Compared to our most complex simulation (2 km resolution and with tides), coarsening the horizontal resolution or deactivating tides (not shown) leads to a warmer continental shelf with similar regional changes. It appears that a poor representation of tides causes overestimated heat transport onto the shelf or underestimated heat loss out of the shelf ocean. The latter could be caused by decreased heat loss to the surface or a

spuriously low conversion rate of heat into ice shelf melting. These findings stress the importance of resolving tides at 4 km
335   horizontal resolution or finer in large-scale models.

Quantifying changes in the heat budget of the continental shelf ocean and determining the exact tidal mechanism responsible
for the model behaviour will require future studies. We hypothesise, however, that vertical mixing on the continental shelf due
to internal tide breaking could play an important role. This is based on the following. First, by means of a high resolution
circum-Antarctic simulation, Stewart et al. (2018) conclude that tide driven exchanges across the continental shelf break are
340   mostly balanced by mean flow, and, second, the generation of internal tides is sensitive to horizontal model resolution with
4 km being sufficient to resolve the most critical aspects (Robertson, 2006; Padman et al., 2006).

WAOM underestimates melting for some ice shelves and we speculate boundary conditions to be the cause. A cold bias
in the Amundsen-Bellingshausen Seas is a common issue in large scale models (e.g. Naughten et al., 2018b) and has been
attributed to, either, insufficient transport of deep ocean heat onto the continental shelf (as mentioned earlier), insufficient
345   transport of onshelf heat into the sub-ice shelf cavities or underestimated conversion efficiency of heat into melting inside
the cavity (Nakayama et al., 2014; Dinniman et al., 2015). In our simulation, onshelf ocean temperatures in the Amundsen-
Bellingshausen Seas are comparable to observations and where deep warm water intrusions reach the ice shelf cavities melt
rates also agree (e.g. for George V and Abbot). Therefore, we expect insufficient transport of onshelf heat into the cavities to be
the cause of underestimated melt rates in the model (e.g. for the ice shelves Pine Island, Getz and Totten, compared to Rignot
350   et al., 2013; Depoorter et al., 2013; Liu et al., 2015). There are a multitude of mechanisms that could prevent onshelf heat from
entering the cavity and that could vary between regions. For example, at Pine Island Ice Shelf, Davis et al. (2018) shows that
local wind forcing modulates thermocline depth, which in turn controls the access of CDW into the cavity on weekly to monthly
timescales. We do not account for the effect of sea ice on surface wind stress in the model and, thus, a bias in thermocline depth
might cause low melting in this region. In contrast, for Totten and Moscow University Ice Shelves we attribute underestimated
355   heat flux into the cavity mostly to a bathymetry bias. A regional model by Gwyther et al. (2014) resolves similar continental
shelf temperatures, but uses a cavity thickness which is 5 times larger along the centreline compared to Bedmap2, and this
model resolves melt rates comparable to satellite estimates.

We consider unresolved sea ice-ocean interactions as the major limitation of WAOM. The ocean connects ice shelf melting
and sea ice in a complex manner (Hellmer, 2004; Padman et al., 2018), having motivated many previous studies to include sea
360   ice models (e.g. Hellmer, 2004; Timmermann et al., 2012; Naughten et al., 2018b). This study, however, prioritises accurate
polynyas by prescribing surface fluxes from sea ice observations. While this is likely to result in more accurate melt rates at
the base of the ice shelves, WAOM can not be used to study processes for which sea ice interaction is critical. Future efforts
aiming to use WAOM for simulating periods beyond the observational record will need to incorporate a dynamic sea ice model
or carefully prescribe surface flux anomalies.

365   The many wasted land cells in WAOM's domain could also be considered a limitation, but the model design simplifies future
coupling with models of ice sheet flow. WAOM's curvilinear grid using a south polar projection necessitates masking of more
than one third of all computational cells, wasting valuable resources with the model integration timestep. This design, however,
has been chosen to simplify future efforts that aim to couple WAOM with models of Antarctic ice sheet flow (e.g. Jong et al.,

2017), as these coupled models are ultimately needed to improve sea level rise predictions (e.g. Colleoni et al., 2018). Also
370 in regards to coupling, ROMS includes routines to resolve sediment transport and passive tracers (see, e.g. Dinniman et al.,
2003; Sherwood et al., 2018, for applications) and activating these options in WAOM will likely be of interest for geological
and biological studies.

To further improve the accuracy of WAOM, future development should focus on the following aspects.

– Establishing an evaluation matrix for circum-Antarctic ice shelf-ocean models would open the path for efficient param-
375 eter tuning (similar to Nakayama et al., 2017) and allow the community to compare the performance between different
models (see Naughten et al., 2018b). Many kinds of observations are useful for this, including ice shelf basal melting
from phase-sensitive radar (ApRES), as well as ocean measurements from Conductivity(Salinity)-Temperature-Depth
(CTD) sensors, Acoustic Doppler Current Profilers (ADCP) and turbulence measurement packages. These ocean in-
struments can be mounted on Autonomous Underwater Vehicles (AUVs) with under ice capability, underwater gliders,
380 drifting floats, moorings and Seals. When rating the model performance against such observations, uncertainties of the
underlying methods and the spatial and temporal variability of the observed quantities must be carefully considered.

ApRES seems particularly suitable for large scale model evaluation as it comprises a robust and cheap method to observe
basal melt rates over longer time periods. As more ApRES measurements are becoming available, their compilation could
provide the backbone for such an evaluation matrix, similar to tide gauge measurements for tidal accuracy (King and
385 Padman, 2005). Comparison of a wide array of ApRES data is already underway with the NECKLACE programme[1].

– Future field campaigns should be guided by model results. To explain why WAOM underestimates the heat flux into
the cavities of some of the warm water ice shelves (Pine Island, Getz, combined Brunt and Riiser-Larsen, Shackleton,
combined Totten and Moscow University), more ocean measurements, including bathymetry, should be taken near the
front of these ice shelves. Also, ApRES measurements are particularly valuable where high resolution satellite estimates
390 have their greatest uncertainties, that is in calving regions and close to grounding lines. Although, crevasses are often
present in these regions and can impede the successful interpretation of ApRES results.

– Accurate bathymetry on the open continental shelf and inside the sub-ice shelf cavities is essential to resolve warm water
intrusions, critical for ice shelf melting and consequent melt water export. Thus, the model bathymetry should be updated
according to regional surveys (e.g. Millan et al., 2017; Nash, 2019).

395 – Studying individual aspects of the model will help gain trust in quantitative results. Schnaase and Timmermann (2019),
for example, show that artificially deepening the water column thickness near grounding zones (necessary for numerical
stability), does not affect ice shelf average melt rates, and Malyarenko et al. (2019) suggest that the unrealistic ice front
representation in sigma-coordinates, could actually account for unresolved small scale processes. Wind stress has been
shown to impact ice shelf melting (Davis et al., 2018; Greene et al., 2017), but how sea ice modulates momentum flux
400 from the atmosphere into the ocean is still an open question (Lüpkes and Birnbaum, 2005; Nøst et al., 2011).

---

[1]NECKLACE programme: http://www.soos.aq/news/current-news/330-necklace-workshop-update.

- The number of wasted land cells in WAOM could be reduced by applying nested grids with coarser resolution in ice sheet areas.

- Finally, including parallel input-output in WAOM would allow for efficient parallelisation at 2 km resolution. The gain in computational cost might make longer simulation periods feasible or allow for a further increase in horizontal resolution
405 until continental shelf quantities converge.

We propose the following experiments to harness the strengths of WAOM.

- Deactivating tides in the model would lead to a first estimate of the impact of tides on Antarctic-wide ice shelf melting and can likely be used to gain further insights into the mechanisms governing tidal melt.

- Experiments that trace individual water masses, such as ISW or AASW, could be used to study the role of ice shelf
410 teleconnections in a pan-Antarctic context or attribute ice shelf mass loss to the individual melting modes.

- Repeating the resolution experiment introduced in this study, but, successively deactivating tides and keeping the bathymetry resolution constant, would unravel the impact of grid spacing on shoreward heat flux from tides, eddies and bathymetry.

- Finally, applying anomalies from future climate projections to the boundary forcing (e.g. from CMIP5; Taylor et al., 2011) could be used to study the response of Antarctic ice shelf melting to warming oceans. This experiment would not
415 just add another estimate that complements other model results by Naughten et al. (2018b), but offers valuable sample points of the average behaviour of the ice shelf cavity system.

5 Summary and Conclusion

Here, we present the Whole Antarctic Ocean Model (WAOM v.1.0). WAOM overcomes two major shortcomings of previous circum-Antarctic ocean-ice shelf models by the inclusion of tides and a horizontal resolution which is high enough to resolve
420 critical shoreward heat transport by eddies (e.g. Dinniman et al., 2016). We have simulated present day conditions by spinning up the model to a quasi equilibrium with repeated 2007-forcing.

Model results compare well against available observations. Continental shelf ocean temperatures and ice shelf melting converge with increasing model resolution, but a further refinement to 1 km grid spacing is likely needed to reach asymptotic behaviour. The accuracy of tidal height signals at the coast is comparable to state-of-the-art barotropic tide models and the
425 off-shelf hydrography agrees well with SOSE, which assimilates most of the available observations in the Southern Ocean. On the continental shelf, where observations are sparse, WAOM resolves realistic hydrography, e.g., featuring bottom layer temperatures of 1 °C in the Amundsen-Bellingshausen Seas and WDW in the Weddell Sea. Ice shelf melting and marine ice accretion at high resolution show that WAOM captures the known modes of melting, often in agreement with regional studies. Ice shelf average melt rates agree with satellite observations at many places, but indicate a cold bias for some of the warm
430 water ice shelves in the Amundsen-Bellingshausen Seas as well as the Totten and Moscow-University Ice Shelf System. We

attribute these discrepancies to insufficient heat flux from the continental shelf into the sub-ice shelf cavities, likely due to regional uncertainties in bathymetry or wind stress.

To further improve WAOM, future studies should mostly focus on compiling available observations of ice-ocean interaction around Antarctica. Efforts are underway to collect all available ApRES measurements of ice shelf basal melting around
435 Antarctica (the NECKLACE programme) and this could form the base for a consistent evaluation matrix of large scale ice shelf-ocean models. Such a framework would not just help to tune model parameters in an efficient manner, but also compare the performance between different models and, thus, focus community model development. Further, the bathymetry in WAOM should be updated where regional products are available and future studies should target individual, uncertain aspects in the model, such as how sea ice modulates wind stress and the representation of surface water advection under the ice front.

440 Resolving ice shelf-ocean interaction at high resolution is the main purpose of WAOM. The only available estimate of Antarctic-wide ice shelf basal melting at high resolution has been derived from satellite observations and models of surface processes with unknown uncertainty (Rignot et al., 2013). Thus, new estimates derived from a fully independent method, that also offers an ocean consistent to the melt rates, is likely to result in new insights into the governing processes that drive Antarctic ice shelf melting. Further, WAOM is well suited for giving a first estimate of circum-Antarctic tidal melting and to
445 explore the average behaviour of all ice shelf cavity systems found around the continent. WAOM is not coupled to a dynamic sea ice model and, thus, future simulations will need estimates of sea ice-ocean fluxes from climate models. Alternatively, WAOM could be coupled to a sea ice model, in a manner similar to Naughten et al. (2018b).

To reduce uncertainties in predictions of future sea level rise and climate, models will ultimately need to resolve interaction between the Antarctic ice sheet and the Southern Ocean over glaciological timescales (e.g. Colleoni et al., 2018). Code that
450 communicates the shared properties between ice sheet and ocean models is now available (Jong et al., 2017), and idealized and regional applications with ROMS show promising results (as discussed in Asay-Davis et al., 2017). WAOM has been designed to provide the ocean component of a coupled Antarctic-wide application and this study presented development and evaluation of a present day simulation and is a major step towards this goal.

Code and data availability. The model output can be obtained from the authors upon request. The source code and configuration files used
455 for the simulations described here are archived at http://doi.org/10.5281/zenodo.3738985 (Richter, 2020a), while the maintained version is publicly available at https://github.com/kuechenrole/waom. The grid files, atmospheric forcing, initial conditions, and northern boundary conditions can be obtained from the authors upon request. The Python and Matlab scripts used to generate the grid and forcing files and to perform the analysis on the model output are archived at http://doi.org/10.5281/zenodo.3738998 (Richter, 2020b) and the maintained version of these scripts is publicly available at https://github.com/kuechenrole/antarctic_melting.

460 **Appendix A: Antarctic Ice Shelf Melting From Observations and Models**

Geoscientific Model Development — Discussions — Open Access — EGU

Table A1. Antarctic ice shelf basal mass loss from models and satellite observations. Results for this study have been calculated using ice shelf boundaries from the MEaSUREs Antarctic boundaries dataset (Mouginot et al., 2016) or Bedmap2 (Fretwell et al., 2013). Other modelling studies are Hellmer (2004); Timmermann et al. (2012); Dinniman et al. (2015); Schodlok et al. (2016); Mathiot et al. (2017); Naughten et al. (2018b) and studies using satellite observations and models of surface processes are Rignot et al. (2013); Depoorter et al. (2013); Liu et al. (2015). Among the satellite studies, only Liu et al. (2015) avoids the assumption of a steady state calving front when inferring basal conditions (referred to as Liu 2015 (non steady); see Liu et al., 2015). Rignot 2013 (hr data) estimates have been calculated by integrating the high resolution solution from Rignot et al. (2013) and using MEaSUREs ice shelf boundaries. Naughten et al. (2018b) and Mathiot et al. (2017) area average melt rates for individual ice shelves have been calculated using area definitions from Rignot et al. (2013). Abbreviations are melt rate (w_b) and Basal Mass Loss (BML).

BML (Gt/yr) / w_b (m/yr) / Area (10^3 km^2)		This study (MEaSUREs)	This study (Bedmap2)	Rignot 2013 (IS flux)	error	Rignot 2013 (hr data)	Liu 2015 (non steady)	error	Liu 2015 (steady state)	error	Depoorter 2013	error	Hellmer 2004	Timmermann 2012	Dinniman 2015	Schodlok 2016	Mathiot 2017	Naughten 2018 (MetROMS)	Naughten 2018 (FESOM HR)
Total Antarctica	BML	973.34	1209.10	1500.00	237.00	1046.31	1516.00	106.00	1290.00	110.00	1454.00	174.00	906.60	1600.00	664.00	1735.00	1864.00	642.00	739.00
	w_b	0.70	0.82	0.85	0.10	0.75	1.10	0.10	0.90	0.10	0.94	0.11	0.80	1.20	-	1.16		0.52	0.56
	Area	1523.33	1617.62	1561.40		1529.46	1542.11		1542.11		1555.00		1233.00	1510.00	-	1625.00		1349.00	1438.00
Amery	BML	10.56	10.03	35.50	23.00	40.38	95.00	8.00	63.00	9.00	39.00	21.00	17.65	174.00			207.00	91.00	71.40
	w_b	0.19	0.18	0.58	0.40	0.77	1.70	0.10	1.10	0.20	1.10	0.35	0.35	2.90	1.10	1.25	3.73	1.64	1.29
	Area	59.13	60.53	60.65		57.53	62.23		62.23		60.00		55.00	67.00			60.65	60.65	60.65
Totten & Moscow Uni.	BML	13.26	18.39	90.60	8.00	67.50	122.00	12.00	90.00	12.00	92.00	19.00						9.50	9.30
	w_b	1.25	1.52	7.66	0.73	7.29	10.68	1.02	7.86	1.02	7.41	1.62				2.06		0.88	0.86
	Area	11.60	13.23	11.83		10.10	12.55		12.55		12.00							11.83	11.83
Shackleton	BML	17.12	23.63	72.60	15.00	55.21	96.00	7.00	60.00	7.00	76.00	23.00	47.68				14.00	14.30	17.40
	w_b	0.74	0.88	2.78	0.60	2.50	3.39	0.26	2.14	0.26	2.20	0.67	1.04			0.52	0.59	0.60	0.73
	Area	25.26	29.21	26.08		24.12	31.04		31.04		35.00		50.00				26.08	26.08	26.08
Ross	BML	66.48	69.10	47.70	34.00	27.50	27.00	22.00	71.00	25.00	34.00	25.00	180.20	260.00			111.00	53.80	112.00
	w_b	0.15	0.15	0.10	0.10	0.06	0.10	0.00	0.20	0.10	0.07	0.05	0.49	0.60	0.14	0.36	0.24	0.12	0.24
	Area	490.40	493.61	500.81		485.39	497.78		497.81		477.00		401.00	475.00			500.81	500.81	500.81
Larsen C**	BML	9.08	13.12	20.70	67.00	5.46	55.00	7.00	6.00	8.00	18.00	8.00	38.13	48.00			46.00	18.20	54.70
	w_b	0.22	0.26	0.45	1.00	0.13	1.00	0.10	0.10	0.20	0.30	0.14	0.63	1.00	0.35	1.47	1.08	0.43	1.29
	Area	45.62	55.66	46.47		44.39	57.04		57.04		60.00		66.00	52.00			46.47	46.47	46.47
Filchner-Ronne	BML	90.25	87.09	155.40	43.00	127.66	10.00	32.00	82.00	37.00	50.00	40.00	119.70	138.00			123.00	46.00	115.40
	w_b	0.23	0.22	0.32	0.10	0.33	0.00	0.10	0.20	0.10	0.12	0.09	0.32	0.35	0.19	0.25	0.30	0.11	0.28
	Area	433.32	433.95	443.14		426.51	426.35		426.35		423.00		408.00	438.00			443.14	443.14	443.14
Brunt + Riiser-Larsen	BML	64.53	68.45	9.70	14.00	11.05	20.00	10.00	37.10	10.00	26.00	16.00	165.90	65.00			39.00	29.20	34.60
	w_b	0.89	0.93	0.12	0.20	0.16	0.25	0.12	0.50	0.14	0.33	0.20	2.38	0.94	0.67	0.28	0.53	0.40	0.47
	Area	78.86	80.65	80.34		76.66	81.84		81.84		79.00		76.00	77.00			80.34	80.34	80.34
Fimbulisen & Jelbart*	BML	62.94	67.39	22.50	12.00	14.31	55.10	11.00	46.00	11.00	24.00	13.00	243.10	130.00			39.00	30.30	52.40
	w_b	1.36	1.41	0.43	0.22	0.32	0.75	0.12	0.62	0.15	0.52	0.27	4.91	2.80	1.51	1.16	0.82	0.64	1.11
	Area	50.54	52.20	51.69		48.81	78.06		78.06		46.00		54.00	53.00			51.69	51.69	51.69
Getz	BML	60.12	67.13	144.90	13.00	120.91	149.00	16.00	96.00	16.00	136.00	23.00	53.64	164.00			337.00	88.10	30.60
	w_b	1.99	2.04	4.26	0.40	4.22	4.80	0.50	3.10	0.50	4.09	0.68	1.95	5.40	0.66	11.05	10.81	2.83	0.98
	Area	33.05	35.86	34.02		31.31	33.74		33.74		33.00		30.00	35.00			34.02	34.02	34.02
Pine Island	BML	36.65	41.18	101.20	8.00	85.96	78.00	8.00	51.00	8.00	95.00	14.00		13.00			87.00	20.50	9.50
	w_b	7.03	7.28	16.20	0.10	17.75	14.00	1.40	9.10	1.40	15.96	2.38		3.10	1.62	14.91	15.20	3.58	1.66
	Area	5.69	6.18	6.25		5.29	6.09		6.09		6.00			5.00			6.25	6.25	6.25
Abbot	BML	73.63	80.93	51.80	20.00	38.56	35.00	7.00	46.00	7.00	86.00	22.00	18.60	59.00			52.00	25.00	36.60
	w_b	2.60	2.65	1.75	0.60	1.47	1.20	0.20	1.60	0.20	2.72	0.70	0.55	2.10	0.34	1.23	1.91	0.92	1.35
	Area	30.90	33.37	29.69		28.70	32.51		32.51		32.00		36.00	32.50			29.69	29.69	29.69
George VI**	BML	145.59	152.31	89.00	17.00	63.20	76.00	13.00	56.00	13.00	144.00	42.00	22.48	86.00			298.00	48.40	32.50
	w_b	6.99	7.06	3.80	0.70	3.20	4.02	0.73	2.94	0.67	2.88	0.83	0.43	3.60	1.19	7.99	13.88	2.25	1.51
	Area	22.79	23.50	23.43		21.56	20.59		20.59		50.00		57.00	27.00			23.43	23.43	23.43

* Liu et al. (2015) also includes Vigrid, Nivil, Lazarev, Borchgrevink.

** Depoorter et al. (2013) also includes Larsen B.

*** Depoorter et al. (2013) and Hellmer (2004) includes Wilkens and Stange.

Appendix B: Computational Ice Shelf Masks

Figure B1. Difference in ice area definition. Red areas show ice that is excluded when imposing ice shelf boundaries from the MEaSURES Antarctic Boundaries data set (Mouginot et al., 2016) onto the ice draft from Bedmap2 (Fretwell et al., 2013).

Appendix C: Model Configuration

Table C1. Activated ROMS options in WAOM.

Category	CPP option	Description
Momentum equations	UV_COR	Coriolis term
	UV_VIS2	harmonic horizontal mixing
	UV_QDRAG	quadratic bottom friction
	UV_ADV	advection terms
	MIX_S_UV	mixing along constant S-surfaces
	SPLINES_VVISC	splines reconstruction of vertical viscosity
pressure gradient	DJ_GRADPS	splines density Jacobian
Tracer equations	TS_A4HADVECTION	4th-order Akima horizontal advection
	TS_A4VADVECTION	4th-order Akima vertical advection
	TS_DIF2	harmonic horizontal mixing
	SALINITY	having salinity
	MIX_ISO_TS	mixing on epineutral (constant RHO) surfaces
	NONLIN_EOS	nonlinear equation of state
	QCORRECTION	net heat flux correction
	SCORRECTION	freshwater flux correction
	SURFACE_OVERFLUX_FIX	corrections for not having a sea ice model
Vertical mixing	LMD_MIXING	Large et al. (1994) interior closure
	LMD_CONVEC	add convective mixing due to shear instability
	RI_SPLINES	splines reconstruction for Richardson Number
	LMD_DDMIX	double-diffusive mixing
	LMD_RIMIX	add diffusivity due to shear instability
	LMD_SKPP	surface boundary layer KPP mixing
	LMD_BKPP	bottom boundary layer KPP mixing
	LMD_NONLOCAL	nonlocal transport
	LMD_SHAPIRO	shapiro filtering boundary layer depth
Bottom stress	LIMIT_BSTRESS	limit the magnitude of bottom stress
Model configuration	SOLVE3D	3D primitive equations
	CURVGRID	curvilinear coordinates grid
	SPHERICAL	spherical grid
	AVERAGES	writing out NLM time-averaged data
	MASKING	land/sea masking
Analytical fields	ANA_BSFLUX	analytical bottom salinity flux
	ANA_BTFLUX	analytical bottom temperature flux
	ANA_SRFLUX	analytical surface shortwave radiation flux
	SPLINES_VDIFF	splines reconstruction of vertical diffusion
Ice shelf	ICESHELF	including ice shelf cavities
	LIMIT_ICESTRESS	limit the magnitude of ice shelf basal stress
	ICESHELF_3EQN_VBC	activate 3-equation ice/ocean thermodynamics
Tides	SSH_TIDES	imposing tidal elevation
	ADD_FSOBC	add tidal elevation to processed OBC data
	UV_TIDES	imposing tidal currents
	ADD_M2OBC	add tidal currents to processed OBC data
	RAMP_TIDES	ramping (over one day) tidal forcing
NetCDF input/output	PERFECT_RESTART	include perfect restart variables

Table C2. Some key model parameters.

Parameter	value (10/4/2 km resolution)
Vertical resolution (# layers)	31
Vertical coordinate transformation equation #	2
Vertical coordinate transformation stretching function #	4
Surface stretching parameter	7
Bottom stretching parameter	8
Critical depth (m)	250
Baroclinic timestep (s)	900/360/180
Barotropic timestep (s)	25/10/5
Horizontal diffusivity ($m^2 s^{-1}$)	50/20/10
Horizontal viscosity ($m^2 s^{-1}$)	500/200/100
Tracer relaxation time scale (days)	365
Surface elevation relaxation time scale (days)	3
Barotropic momentum relaxation time scale (days)	3
Baroclinic momentum relaxation time scale (days)	3
Open boundary outflow/inflow nudging factor	365

Author contributions. Ole Richter and Benjamin K. Galton-Fenzi conceived and designed the experiments. Ole Richter performed the simulations. Ole Richter, Benjamin K. Galton-Fenzi and David E. Gwyther analysed the data, whereby Kaitlin A. Naughten contributed analysis
465 tools. Ole Richter prepared the manuscript with contributions from all co-authors.

Competing interests. The authors declare that they have no conflict of interest.

Acknowledgements. This research was supported by scholarships from the Australian Government and the Australian Research Council's
Special Research Initiative for the Antarctic Gateway Partnership SRI40300001. Computational resources were provided by the NCI National
Facility at the Australian National University, through awards under the Merit Allocation Scheme. We would like to thank Eric Rignot and
470 Jeremie Mouginot for providing us with the satellite derived melt rates. We are also grateful to Richard Coleman for his valuable comments
on the manuscript and Just Berkhout for his excellent IT support.

References

Asay-Davis, X. S., Jourdain, N. C., and Nakayama, Y.: Developments in Simulating and Parameterizing Interactions Between the Southern Ocean and the Antarctic Ice Sheet, Current Climate Change Reports, 3, 316–329, https://doi.org/10.1007/s40641-017-0071-0, https://link. springer.com/article/10.1007/s40641-017-0071-0, 2017.

Assmann, K. M., Jenkins, A., Shoosmith, D. R., Walker, D. P., Jacobs, S. S., and Nicholls, K. W.: Variability of Circumpolar Deep Water transport onto the Amundsen Sea Continental shelf through a shelf break trough, Journal of Geophysical Research: Oceans, 118, 6603–6620, https://doi.org/10.1002/2013JC008871, https://agupubs.onlinelibrary.wiley.com/doi/abs/10.1002/2013JC008871, 2013.

Colleoni, F., Santis, L. D., Siddoway, C. S., Bergamasco, A., Golledge, N. R., Lohmann, G., Passchier, S., and Siegert, M. J.: Spatio-temporal variability of processes across Antarctic ice-bed–ocean interfaces, Nature Communications, 9, 2289, https://doi.org/10.1038/s41467-018-04583-0, https://www.nature.com/articles/s41467-018-04583-0, 2018.

Cougnon, E. A., Galton-Fenzi, B. K., Meijers, A. J. S., and Legrésy, B.: Modeling interannual dense shelf water export in the region of the Mertz Glacier Tongue (1992–2007), Journal of Geophysical Research: Oceans, 118, 5858–5872, https://doi.org/10.1002/2013JC008790, https://agupubs.onlinelibrary.wiley.com/doi/abs/10.1002/2013JC008790, 2013.

Davis, P. E. D., Jenkins, A., Nicholls, K. W., Brennan, P. V., Abrahamsen, E. P., Heywood, K. J., Dutrieux, P., Cho, K.-H., and Kim, T.-W.: Variability in Basal Melting Beneath Pine Island Ice Shelf on Weekly to Monthly Timescales, Journal of Geophysical Research: Oceans, 123, 8655–8669, https://doi.org/10.1029/2018JC014464, https://agupubs.onlinelibrary.wiley.com/doi/abs/10.1029/2018JC014464, 2018.

Dee, D. P., Uppala, S. M., Simmons, A. J., Berrisford, P., Poli, P., Kobayashi, S., Andrae, U., Balmaseda, M. A., Balsamo, G., Bauer, P., Bechtold, P., Beljaars, A. C. M., Berg, L. v. d., Bidlot, J., Bormann, N., Delsol, C., Dragani, R., Fuentes, M., Geer, A. J., Haimberger, L., Healy, S. B., Hersbach, H., Hólm, E. V., Isaksen, L., Kållberg, P., Köhler, M., Matricardi, M., McNally, A. P., Monge-Sanz, B. M., Morcrette, J.-J., Park, B.-K., Peubey, C., Rosnay, P. d., Tavolato, C., Thépaut, J.-N., and Vitart, F.: The ERA-Interim reanalysis: configuration and performance of the data assimilation system, Quarterly Journal of the Royal Meteorological Society, 137, 553–597, https://doi.org/10.1002/qj.828, https://rmets.onlinelibrary.wiley.com/doi/abs/10.1002/qj.828, 2011.

Depoorter, M. A., Bamber, J. L., Griggs, J. A., Lenaerts, J. T. M., Ligtenberg, S. R. M., van den Broeke, M. R., and Moholdt, G.: Calving fluxes and basal melt rates of Antarctic ice shelves, Nature, 502, 89–92, https://doi.org/10.1038/nature12567, https://www.nature.com/articles/nature12567, 2013.

Dinniman, M. S., Klinck, J. M., and Smith, W. O.: Cross-shelf exchange in a model of the Ross Sea circulation and biogeochemistry, Deep Sea Research Part II: Topical Studies in Oceanography, 50, 3103–3120, https://doi.org/10.1016/j.dsr2.2003.07.011, http://www.sciencedirect.com/science/article/pii/S0967064503001826, 2003.

Dinniman, M. S., Klinck, J. M., Bai, L.-S., Bromwich, D. H., Hines, K. M., and Holland, D. M.: The Effect of Atmospheric Forcing Resolution on Delivery of Ocean Heat to the Antarctic Floating Ice Shelves, Journal of Climate, 28, 6067–6085, https://doi.org/10.1175/JCLI-D-14-00374.1, https://journals.ametsoc.org/doi/full/10.1175/JCLI-D-14-00374.1, 2015.

Dinniman, M. S., Asay-Davis, X. S., Galton-Fenzi, B. K., Holland, P. R., Jenkins, A., and Timmermann, R.: Modeling Ice Shelf/Ocean Interaction in Antarctica: A Review, Oceanography, 29, 144–153, https://doi.org/10.5670/oceanog.2016.106, https://tos.org/oceanography/article/modeling-ice-shelf-ocean-interaction-in-antarctica-a-review, 2016.

Dupont, T. K. and Alley, R. B.: Assessment of the importance of ice-shelf buttressing to ice-sheet flow, Geophysical Research Letters, 32, https://doi.org/10.1029/2004GL022024, https://agupubs.onlinelibrary.wiley.com/doi/abs/10.1029/2004GL022024, 2005.

Dutrieux, P., Vaughan, D. G., Corr, H. F. J., Jenkins, A., Holland, P. R., Joughin, I., and Fleming, A. H.: Pine Island glacier ice shelf
melt distributed at kilometre scales, The Cryosphere, 7, 1543–1555, https://doi.org/https://doi.org/10.5194/tc-7-1543-2013, https://www.
510   the-cryosphere.net/7/1543/2013/, 2013.

Egbert, G. D. and Erofeeva, S. Y.: Efficient Inverse Modeling of Barotropic Ocean Tides, Journal of Atmospheric and Oceanic Technol-
ogy, 19, 183–204, https://doi.org/10.1175/1520-0426(2002)019<0183:EIMOBO>2.0.CO;2, https://journals.ametsoc.org/doi/full/10.1175/
1520-0426%282002%29019%3C0183%3AEIMOBO%3E2.0.CO%3B2, 2002.

Fretwell, P., Pritchard, H. D., Vaughan, D. G., Bamber, J. L., Barrand, N. E., Bell, R., Bianchi, C., Bingham, R. G., Blankenship, D. D.,
515   Casassa, G., Catania, G., Callens, D., Conway, H., Cook, A. J., Corr, H. F. J., Damaske, D., Damm, V., Ferraccioli, F., Forsberg, R.,
Fujita, S., Gim, Y., Gogineni, P., Griggs, J. A., Hindmarsh, R. C. A., Holmlund, P., Holt, J. W., Jacobel, R. W., Jenkins, A., Jokat,
W., Jordan, T., King, E. C., Kohler, J., Krabill, W., Riger-Kusk, M., Langley, K. A., Leitchenkov, G., Leuschen, C., Luyendyk, B. P.,
Matsuoka, K., Mouginot, J., Nitsche, F. O., Nogi, Y., Nost, O. A., Popov, S. V., Rignot, E., Rippin, D. M., Rivera, A., Roberts, J.,
Ross, N., Siegert, M. J., Smith, A. M., Steinhage, D., Studinger, M., Sun, B., Tinto, B. K., Welch, B. C., Wilson, D., Young, D. A.,
520   Xiangbin, C., and Zirizzotti, A.: Bedmap2: improved ice bed, surface and thickness datasets for Antarctica, The Cryosphere, 7, 375–393,
https://doi.org/https://doi.org/10.5194/tc-7-375-2013, https://www.the-cryosphere.net/7/375/2013/, 2013.

Gade, H. G.: Melting of Ice in Sea Water: A Primitive Model with Application to the Antarctic Ice Shelf and Icebergs,
http://dx.doi.org/10.1175/1520-0485(1979)009<0189:MOIISW>2.0.CO;2,   https://journals.ametsoc.org/doi/abs/10.1175/1520-0485%
281979%29009%3C0189%3AMOIISW%3E2.0.CO%3B2, 1979.

525   Galton-Fenzi, B. K., Hunter, J. R., Coleman, R., Marsland, S. J., and Warner, R. C.: Modeling the basal melting and marine ice accretion of
the Amery Ice Shelf, Journal of Geophysical Research: Oceans, 117, https://doi.org/10.1029/2012JC008214, https://agupubs.onlinelibrary.
wiley.com/doi/abs/10.1029/2012JC008214, 2012.

Greene, C. A., Blankenship, D. D., Gwyther, D. E., Silvano, A., and Wijk, E. v.: Wind causes Totten Ice Shelf melt and acceleration, Science
Advances, 3, https://doi.org/10.1126/sciadv.1701681, http://advances.sciencemag.org/content/3/11/e1701681, 2017.

530   Griffiths, S. D. and Peltier, W. R.: Megatides in the Arctic Ocean under glacial conditions, Geophysical Research Letters, 35,
https://doi.org/10.1029/2008GL033263, https://agupubs.onlinelibrary.wiley.com/doi/abs/10.1029/2008GL033263, 2008.

Gudmundsson, G. H.: Ice-shelf buttressing and the stability of marine ice sheets, The Cryosphere, 7, 647–655,
https://doi.org/https://doi.org/10.5194/tc-7-647-2013, https://www.the-cryosphere.net/7/647/2013/, 2013.

Guo, G., Shi, J., Gao, L., Tamura, T., and Williams, G. D.: Reduced Sea Ice Production Due to Upwelled Oceanic Heat Flux in Prydz Bay, East
535   Antarctica, Geophysical Research Letters, 46, 4782–4789, https://doi.org/10.1029/2018GL081463, https://agupubs.onlinelibrary.wiley.
com/doi/abs/10.1029/2018GL081463, 2019.

Gwyther, D. E., Galton-Fenzi, B. K., Hunter, J. R., and Roberts, J. L.: Simulated melt rates for the Totten and Dalton ice shelves, Ocean
Science, 10, 267–279, https://doi.org/https://doi.org/10.5194/os-10-267-2014, https://www.ocean-sci.net/10/267/2014/, 2014.

Gwyther, D. E., Cougnon, E. A., Galton-Fenzi, B. K., Roberts, J. L., Hunter, J. R., and Dinniman, M. S.: Modelling the response of ice shelf
540   basal melting to different ocean cavity environmental regimes, Annals of Glaciology, 57, 131–141, https://doi.org/10.1017/aog.2016.31,
https://www.cambridge.org/core/product/identifier/S0260305516000318/type/journal_article, 2016.

Gwyther, D. E., O'Kane, T. J., Galton-Fenzi, B. K., Monselesan, D. P., and Greenbaum, J. S.: Intrinsic processes drive variability in basal
melting of the Totten Glacier Ice Shelf, Nature Communications, 9, 3141, https://doi.org/10.1038/s41467-018-05618-2, https://www.
nature.com/articles/s41467-018-05618-2, 2018.

545   Hattermann, T.: Antarctic Thermocline Dynamics along a Narrow Shelf with Easterly Winds, Journal of Physical Oceanography, 48, 2419–
2443, https://doi.org/10.1175/JPO-D-18-0064.1, https://journals.ametsoc.org/doi/full/10.1175/JPO-D-18-0064.1, 2018.

Hattermann, T., Nøst, O. A., Lilly, J. M., and Smedsrud, L. H.: Two years of oceanic observations below the Fimbul Ice Shelf, Antarc-
tica, Geophysical Research Letters, 39, https://doi.org/10.1029/2012GL051012, https://agupubs.onlinelibrary.wiley.com/doi/abs/10.1029/
2012GL051012, 2012.

550   Hattermann, T., Smedsrud, L. H., Nøst, O. A., Lilly, J. M., and Galton-Fenzi, B. K.: Eddy-resolving simulations of the Fimbul Ice Shelf cavity
circulation: Basal melting and exchange with open ocean, Ocean Modelling, 82, 28–44, https://doi.org/10.1016/j.ocemod.2014.07.004,
http://www.sciencedirect.com/science/article/pii/S1463500314000948, 2014.

Hellmer, H. H.: Impact of Antarctic ice shelf basal melting on sea ice and deep ocean properties, Geophysical Research Letters, 31,
https://doi.org/10.1029/2004GL019506, https://agupubs.onlinelibrary.wiley.com/doi/abs/10.1029/2004GL019506, 2004.

555   Hellmer, H. H. and Olbers, D. J.: A two-dimensional model for the thermohaline circulation under an ice shelf, Antarctic
Science, 1, 325–336, https://doi.org/10.1017/S0954102089000490, https://www.cambridge.org/core/journals/antarctic-science/article/
twodimensional-model-for-the-thermohaline-circulation-under-an-ice-shelf/DCB7E3D1C510375CD52CBBD6C42A3993#, 1989.

Holland, D. M. and Jenkins, A.: Modeling Thermodynamic Ice–Ocean Interactions at the Base of an Ice Shelf, Journal of Physical Oceanog-
raphy, 29, 1787–1800, https://doi.org/10.1175/1520-0485(1999)029<1787:MTIOIA>2.0.CO;2, https://journals.ametsoc.org/doi/full/10.
560   1175/1520-0485%281999%29029%3C1787%3AMTIOIA%3E2.0.CO%3B2, 1999.

Holland, P. R.: The Transient Response of Ice Shelf Melting to Ocean Change, Journal of Physical Oceanography, 47, 2101–2114,
https://doi.org/10.1175/JPO-D-17-0071.1, https://journals.ametsoc.org/doi/10.1175/JPO-D-17-0071.1, 2017.

Holland, P. R., Feltham, D. L., and Jenkins, A.: Ice Shelf Water plume flow beneath Filchner-Ronne Ice Shelf, Antarctica, Journal of
Geophysical Research, 112, https://doi.org/10.1029/2006JC003915, http://doi.wiley.com/10.1029/2006JC003915, 2007.

565   Holland, P. R., Jenkins, A., and Holland, D. M.: The Response of Ice Shelf Basal Melting to Variations in Ocean Temperature, Journal of
Climate, 21, 2558–2572, https://doi.org/10.1175/2007JCLI1909.1, https://journals.ametsoc.org/doi/full/10.1175/2007JCLI1909.1, 2008.

Holland, P. R., Corr, H. F. J., Vaughan, D. G., Jenkins, A., and Skvarca, P.: Marine ice in Larsen Ice Shelf, Geophysical Research Letters, 36,
https://doi.org/10.1029/2009GL038162, https://agupubs.onlinelibrary.wiley.com/doi/abs/10.1029/2009GL038162, 2009.

Horgan, H. J., Walker, R. T., Anandakrishnan, S., and Alley, R. B.: Surface elevation changes at the front of the Ross Ice Shelf: Implications
570   for basal melting, Journal of Geophysical Research: Oceans, 116, https://doi.org/10.1029/2010JC006192, https://agupubs.onlinelibrary.
wiley.com/doi/abs/10.1029/2010JC006192, 2011.

Jacobs, S. S.: Bottom water production and its links with the thermohaline circulation, Antarctic Science, 16, 427–
437, https://doi.org/10.1017/S095410200400224X, https://www.cambridge.org/core/journals/antarctic-science/article/
bottom-water-production-and-its-links-with-the-thermohaline-circulation/9C29FAEDC0136B2C616B8E7491671916, 2004.

575   Jacobs, S. S., Helmer, H. H., Doake, C. S. M., Jenkins, A., and Frolich, R. M.: Melting of ice shelves and the mass balance of Antarc-
tica, Journal of Glaciology, 38, 375–387, https://doi.org/10.3189/S0022143000002252, https://www.cambridge.org/core/journals/
journal-of-glaciology/article/melting-of-ice-shelves-and-the-mass-balance-of-antarctica/B4841D1BF7AD77C197F8FDA33BE9936C,
1992.

Jacobs, S. S., Jenkins, A., Giulivi, C. F., and Dutrieux, P.: Stronger ocean circulation and increased melting under Pine Island Glacier ice
580   shelf, Nature Geoscience, 4, 519, https://doi.org/10.1038/ngeo1188, https://www.nature.com/articles/ngeo1188, 2011.

Jacobs, S. S., Giulivi, C. F., Dutrieux, P., Rignot, E., Nitsche, F., and Mouginot, J.: Getz Ice Shelf melting response to changes in ocean forcing, Journal of Geophysical Research: Oceans, 118, 4152–4168, https://doi.org/10.1002/jgrc.20298, https://agupubs.onlinelibrary.wiley.com/doi/abs/10.1002/jgrc.20298, 2013.

Jong, L., Gladstone, R., and Galton-Fenzi, B. K.: Coupled ice sheet-ocean modelling to investigate ocean driven melting of marine ice sheets in Antarctica, 19, 1573, http://adsabs.harvard.edu/abs/2017EGUGA..19.1573J, 2017.

Joughin, I. and Padman, L.: Melting and freezing beneath Filchner-Ronne Ice Shelf, Antarctica, Geophysical Research Letters, 30, https://doi.org/10.1029/2003GL016941, https://agupubs.onlinelibrary.wiley.com/doi/abs/10.1029/2003GL016941, 2003.

King, M. A. and Padman, L.: Accuracy assessment of ocean tide models around Antarctica, Geophysical Research Letters, 32, https://doi.org/10.1029/2005GL023901, https://agupubs.onlinelibrary.wiley.com/doi/abs/10.1029/2005GL023901, 2005.

Kusahara, K. and Hasumi, H.: Modeling Antarctic ice shelf responses to future climate changes and impacts on the ocean, Journal of Geophysical Research: Oceans, 118, 2454–2475, https://doi.org/10.1002/jgrc.20166, https://agupubs.onlinelibrary.wiley.com/doi/abs/10.1002/jgrc.20166, 2013.

Large, W. G., McWilliams, J. C., and Doney, S. C.: Oceanic vertical mixing: A review and a model with a nonlocal boundary layer parameterization, Reviews of Geophysics, 32, 363–403, https://doi.org/10.1029/94RG01872, https://agupubs.onlinelibrary.wiley.com/doi/abs/10.1029/94RG01872, 1994.

Little, C. M., Gnanadesikan, A., and Oppenheimer, M.: How ice shelf morphology controls basal melting, Journal of Geophysical Research: Oceans, 114, https://doi.org/10.1029/2008JC005197, https://agupubs.onlinelibrary.wiley.com/doi/abs/10.1029/2008JC005197, 2009.

Liu, Y., Moore, J. C., Cheng, X., Gladstone, R. M., Bassis, J. N., Liu, H., Wen, J., and Hui, F.: Ocean-driven thinning enhances iceberg calving and retreat of Antarctic ice shelves, Proceedings of the National Academy of Sciences, 112, 3263–3268, https://doi.org/10.1073/pnas.1415137112, http://www.pnas.org/content/112/11/3263, 2015.

Lüpkes, C. and Birnbaum, G.: 'Surface Drag in the Arctic Marginal Sea-ice Zone: A Comparison of Different Parameterisation Concepts', Boundary-Layer Meteorology, 117, 179–211, https://doi.org/10.1007/s10546-005-1445-8, https://link.springer.com/article/10.1007/s10546-005-1445-8, 2005.

Mack, S. L., Dinniman, M. S., Klinck, J. M., McGillicuddy, D. J., and Padman, L.: Modeling Ocean Eddies on Antarctica's Cold Water Continental Shelves and Their Effects on Ice Shelf Basal Melting, Journal of Geophysical Research: Oceans, 124, 5067–5084, https://doi.org/10.1029/2018JC014688, https://agupubs.onlinelibrary.wiley.com/doi/abs/10.1029/2018JC014688, 2019.

Makinson, K., Holland, P. R., Jenkins, A., Nicholls, K. W., and Holland, D. M.: Influence of tides on melting and freezing beneath Filchner-Ronne Ice Shelf, Antarctica, Geophysical Research Letters, 38, https://doi.org/10.1029/2010GL046462, https://agupubs.onlinelibrary.wiley.com/doi/abs/10.1029/2010GL046462, 2011.

Malyarenko, A., Robinson, N. J., Williams, M. J. M., and Langhorne, P. J.: A Wedge Mechanism for Summer Surface Water Inflow Into the Ross Ice Shelf Cavity, Journal of Geophysical Research: Oceans, 124, 1196–1214, https://doi.org/10.1029/2018JC014594, https://agupubs.onlinelibrary.wiley.com/doi/abs/10.1029/2018JC014594, 2019.

Mathiot, P., Jenkins, A., Harris, C., and Madec, G.: Explicit representation and parametrised impacts of under ice shelf seas in the z^* coordinate ocean model NEMO 3.6, Geoscientific Model Development, 10, 2849–2874, https://doi.org/https://doi.org/10.5194/gmd-10-2849-2017, https://www.geosci-model-dev.net/10/2849/2017/, 2017.

Mazloff, M. R., Heimbach, P., and Wunsch, C.: An Eddy-Permitting Southern Ocean State Estimate, Journal of Physical Oceanography, 40, 880–899, https://doi.org/10.1175/2009JPO4236.1, https://journals.ametsoc.org/doi/full/10.1175/2009JPO4236.1, 2010.

McPhee, M. G.: A time-dependent model for turbulent transfer in a stratified oceanic boundary layer, Journal of Geophysical Research: Oceans, 92, 6977–6986, https://doi.org/10.1029/JC092iC07p06977, https://agupubs.onlinelibrary.wiley.com/doi/abs/10.1029/JC092iC07p06977, 1987.

Mellor, G. L., Ezer, T., and Oey, L.-Y.: The Pressure Gradient Conundrum of Sigma Coordinate Ocean Models, Journal of Atmospheric and Oceanic Technology, 11, 1126–1134, https://doi.org/10.1175/1520-0426(1994)011<1126:TPGCOS>2.0.CO;2, https://journals.ametsoc.org/doi/10.1175/1520-0426%281994%29011%3C1126%3ATPGCOS%3E2.0.CO%3B2, 1994.

Mellor, G. L., Oey, L.-Y., and Ezer, T.: Sigma Coordinate Pressure Gradient Errors and the Seamount Problem, Journal of Atmospheric and Oceanic Technology, 15, 1122–1131, https://doi.org/10.1175/1520-0426(1998)015<1122:SCPGEA>2.0.CO;2, http://journals.ametsoc.org/doi/abs/10.1175/1520-0426%281998%29015%3C1122%3ASCPGEA%3E2.0.CO%3B2, 1998.

Menemenlis, D., Campin, J., Heimbach, P., Hill, C., Lee, T., Nguyen, A., Schodlok, M., and Zhang, H.: ECCO2: High Resolution Global Ocean and Sea Ice Data Synthesis, AGU Fall Meeting Abstracts, http://adsabs.harvard.edu/abs/2008AGUFMOS31C1292M, 2008.

Millan, R., Rignot, E., Bernier, V., Morlighem, M., and Dutrieux, P.: Bathymetry of the Amundsen Sea Embayment sector of West Antarctica from Operation IceBridge gravity and other data, Geophysical Research Letters, 44, 1360–1368, https://doi.org/10.1002/2016GL072071, https://agupubs.onlinelibrary.wiley.com/doi/abs/10.1002/2016GL072071, 2017.

Mouginot, J., Rignot, E., and Scheuchl, B.: MEaSURES Antarctic Boundaries for IPY 2007-2009 from Satellite Radar, Version 1. Shelves, http://dx.doi.org/10.5067/SEVV4MR8P1ZN., 2016.

Mueller, R. D., Padman, L., Dinniman, M. S., Erofeeva, S. Y., Fricker, H. A., and King, M. A.: Impact of tide-topography interactions on basal melting of Larsen C Ice Shelf, Antarctica, Journal of Geophysical Research: Oceans, 117, https://doi.org/10.1029/2011JC007263, https://agupubs.onlinelibrary.wiley.com/doi/abs/10.1029/2011JC007263, 2012.

Mueller, R. D., Hattermann, T., Howard, S. L., and Padman, L.: Tidal influences on a future evolution of the Filchner–Ronne Ice Shelf cavity in the Weddell Sea, Antarctica, The Cryosphere, 12, 453–476, https://doi.org/https://doi.org/10.5194/tc-12-453-2018, https://www.the-cryosphere.net/12/453/2018/, 2018.

Nakayama, Y., Timmermann, R., Schröder, M., and Hellmer, H. H.: On the difficulty of modeling Circumpolar Deep Water intrusions onto the Amundsen Sea continental shelf, Ocean Modelling, 84, 26–34, https://doi.org/10.1016/j.ocemod.2014.09.007, https://linkinghub.elsevier.com/retrieve/pii/S1463500314001383, 2014.

Nakayama, Y., Menemenlis, D., Schodlok, M., and Rignot, E.: Amundsen and Bellingshausen Seas simulation with optimized ocean, sea ice, and thermodynamic ice shelf model parameters, Journal of Geophysical Research: Oceans, 122, 6180–6195, https://doi.org/10.1002/2016JC012538, https://agupubs.onlinelibrary.wiley.com/doi/abs/10.1002/2016JC012538, 2017.

Nash, R.: International Bathymetric Chart of the Southern Ocean (IBCSO), https://www.scar.org/science/ibcso/ibcso/, library Catalog: www.scar.org, 2019.

Naughten, K. A., Meissner, K. J., Galton-Fenzi, B. K., England, M. H., Timmermann, R., and Hellmer, H. H.: Future Projections of Antarctic Ice Shelf Melting Based on CMIP5 Scenarios, Journal of Climate, 31, 5243–5261, https://doi.org/10.1175/JCLI-D-17-0854.1, https://journals.ametsoc.org/doi/10.1175/JCLI-D-17-0854.1, 2018a.

Naughten, K. A., Meissner, K. J., Galton-Fenzi, B. K., England, M. H., Timmermann, R., Hellmer, H. H., Hattermann, T., and Debernard, J. B.: Intercomparison of Antarctic ice-shelf, ocean, and sea-ice interactions simulated by MetROMS-iceshelf and FESOM 1.4, Geoscientific Model Development, 11, 1257–1292, https://doi.org/https://doi.org/10.5194/gmd-11-1257-2018, https://www.geosci-model-dev.net/11/1257/2018/, 2018b.

655   Nicholls, K. W., Østerhus, S., Makinson, K., Gammelsrød, T., and Fahrbach, E.: Ice-ocean processes over the continental shelf of the southern Weddell Sea, Antarctica: A review, Reviews of Geophysics, 47, https://doi.org/10.1029/2007RG000250, https://agupubs.onlinelibrary.wiley.com/doi/abs/10.1029/2007RG000250, 2009.

Nøst, O. A., Biuw, M., Tverberg, V., Lydersen, C., Hattermann, T., Zhou, Q., Smedsrud, L. H., and Kovacs, K. M.: Eddy over-turning of the Antarctic Slope Front controls glacial melting in the Eastern Weddell Sea, Journal of Geophysical Research:
660   Oceans, 116, https://doi.org/10.1029/2011JC006965, https://agupubs.onlinelibrary.wiley.com/doi/abs/10.1029/2011JC006965, _eprint: https://agupubs.onlinelibrary.wiley.com/doi/pdf/10.1029/2011JC006965, 2011.

Padman, L., Howard, S. L., and Muench, R.: Internal tide generation along the South Scotia Ridge, Deep Sea Research Part II: Topi-cal Studies in Oceanography, 53, 157–171, https://doi.org/10.1016/j.dsr2.2005.07.011, http://www.sciencedirect.com/science/article/pii/S0967064506000130, 2006.

665   Padman, L., Howard, S. L., Orsi, A. H., and Muench, R. D.: Tides of the northwestern Ross Sea and their impact on dense outflows of Antarc-tic Bottom Water, Deep Sea Research Part II: Topical Studies in Oceanography, 56, 818–834, https://doi.org/10.1016/j.dsr2.2008.10.026, http://linkinghub.elsevier.com/retrieve/pii/S0967064508003615, 2009.

Padman, L., Siegfried, M. R., and Fricker, H. A.: Ocean Tide Influences on the Antarctic and Greenland Ice Sheets, Reviews of Geophysics, 56, 142–184, https://doi.org/10.1002/2016RG000546, https://agupubs.onlinelibrary.wiley.com/doi/abs/10.1002/2016RG000546, 2018.

670   Pawlowicz, R., Beardsley, B., and Lentz, S.: Classical tidal harmonic analysis including error estimates in MATLAB using T_TIDE, Com-puters & Geosciences, 28, 929–937, https://doi.org/10.1016/S0098-3004(02)00013-4, http://www.sciencedirect.com/science/article/pii/S0098300402000134, 2002.

Pritchard, H. D., Ligtenberg, S. R. M., Fricker, H. A., Vaughan, D. G., van den Broeke, M. R., and Padman, L.: Antarctic ice-sheet loss driven by basal melting of ice shelves, Nature, 484, 502–505, https://doi.org/10.1038/nature10968, http://www.nature.com/doifinder/10.
675   1038/nature10968, 2012.

Purkey, S. G. and Johnson, G. C.: Antarctic Bottom Water Warming and Freshening: Contributions to Sea Level Rise, Ocean Freshwater Budgets, and Global Heat Gain, Journal of Climate, 26, 6105–6122, https://doi.org/10.1175/JCLI-D-12-00834.1, https://journals.ametsoc.org/doi/10.1175/JCLI-D-12-00834.1, 2013.

Richter, O.: Whole Antarctic Ocean Model, https://doi.org/10.5281/ZENODO.3738985, 2020a.
680   Richter, O.: Post- and preprocessing tools for the ROMS Whole Antarctic Ocean Model, https://doi.org/10.5281/ZENODO.3738998, 2020b.

Rignot, E., Jacobs, S. S., Mouginot, J., and Scheuchl, B.: Ice-Shelf Melting Around Antarctica, Science, 341, 266–270, https://doi.org/10.1126/science.1235798, http://science.sciencemag.org/content/341/6143/266, 2013.

Robertson, R.: Modeling internal tides over Fieberling Guyot: resolution, parameterization, performance, Ocean Dynamics, 56, 430–444, https://doi.org/10.1007/s10236-006-0062-5, https://doi.org/10.1007/s10236-006-0062-5, 2006.

685   Schaffer, J., Timmermann, R., Arndt, J. E., Kristensen, S. S., Mayer, C., Morlighem, M., and Steinhage, D.: A global, high-resolution data set of ice sheet topography, cavity geometry, and ocean bathymetry, Earth System Science Data, 8, 543–557, https://doi.org/https://doi.org/10.5194/essd-8-543-2016, https://www.earth-syst-sci-data.net/8/543/2016/, 2016.

Schmidtko, S., Heywood, K. J., Thompson, A. F., and Aoki, S.: Multidecadal warming of Antarctic waters, Science, 346, 1227–1231, https://doi.org/10.1126/science.1256117, https://science.sciencemag.org/content/346/6214/1227, 2014.

690   Schnaase, F. and Timmermann, R.: Representation of shallow grounding zones in an ice shelf-ocean model with terrain-following coordi-nates, Ocean Modelling, 144, 101 487, https://doi.org/10.1016/j.ocemod.2019.101487, http://www.sciencedirect.com/science/article/pii/S1463500318302956, 2019.

Schodlok, M. P., Menemenlis, D., and Rignot, E.: Ice shelf basal melt rates around Antarctica from simulations and observations, Journal of Geophysical Research: Oceans, 121, 1085–1109, https://doi.org/10.1002/2015JC011117, https://agupubs.onlinelibrary.wiley.com/doi/abs/10.1002/2015JC011117, 2016.

Shean, D. E., Joughin, I. R., Dutrieux, P., Smith, B. E., and Berthier, E.: Ice shelf basal melt rates from a high-resolution DEM record for Pine Island Glacier, Antarctica, The Cryosphere Discussions, pp. 1–39, https://doi.org/https://doi.org/10.5194/tc-2018-209, https://www.the-cryosphere-discuss.net/tc-2018-209/, 2018.

Sherwood, C. R., Aretxabaleta, A. L., Harris, C. K., Rinehimer, J. P., Verney, R., and Ferré, B.: Cohesive and mixed sediment in the Regional Ocean Modeling System (ROMS v3.6) implemented in the Coupled Ocean–Atmosphere–Wave–Sediment Transport Modeling System (COAWST r1234), Geoscientific Model Development, 11, 1849–1871, https://doi.org/https://doi.org/10.5194/gmd-11-1849-2018, https://www.geosci-model-dev.net/11/1849/2018/, 2018.

Sikirić, M. D., Janeković, I., and Kuzmić, M.: A new approach to bathymetry smoothing in sigma-coordinate ocean models, Ocean Modelling, 29, 128–136, https://doi.org/10.1016/j.ocemod.2009.03.009, http://www.sciencedirect.com/science/article/pii/S1463500309000742, 2009.

Silvano, A., Rintoul, S. R., Peña-Molino, B., and Williams, G. D.: Distribution of water masses and meltwater on the continental shelf near the Totten and Moscow University ice shelves, Journal of Geophysical Research: Oceans, 122, 2050–2068, https://doi.org/10.1002/2016JC012115, https://agupubs.onlinelibrary.wiley.com/doi/abs/10.1002/2016JC012115, 2017.

Silvano, A., Rintoul, S. R., Peña-Molino, B., Hobbs, W. R., Wijk, E. v., Aoki, S., Tamura, T., and Williams, G. D.: Freshening by glacial meltwater enhances melting of ice shelves and reduces formation of Antarctic Bottom Water, Science Advances, 4, eaap9467, https://doi.org/10.1126/sciadv.aap9467, http://advances.sciencemag.org/content/4/4/eaap9467, 2018.

Stern, A. A., Dinniman, M. S., Zagorodnov, V., Tyler, S. W., and Holland, D. M.: Intrusion of warm surface water beneath the McMurdo Ice Shelf, Antarctica, Journal of Geophysical Research: Oceans, 118, 7036–7048, https://doi.org/10.1002/2013JC008842, https://agupubs.onlinelibrary.wiley.com/doi/abs/10.1002/2013JC008842, 2013.

Stewart, A. L. and Thompson, A. F.: Eddy-mediated transport of warm Circumpolar Deep Water across the Antarctic Shelf Break, Geophysical Research Letters, 42, 432–440, https://doi.org/10.1002/2014GL062281, https://agupubs.onlinelibrary.wiley.com/doi/10.1002/2014GL062281, 2015.

Stewart, A. L., Klocker, A., and Menemenlis, D.: Circum-Antarctic Shoreward Heat Transport Derived From an Eddy- and Tide-Resolving Simulation, Geophysical Research Letters, 45, 834–845, https://doi.org/10.1002/2017GL075677, https://agupubs.onlinelibrary.wiley.com/doi/abs/10.1002/2017GL075677, 2018.

Stewart, C. L., Christoffersen, P., Nicholls, K. W., Williams, M. J. M., and Dowdeswell, J. A.: Basal melting of Ross Ice Shelf from solar heat absorption in an ice-front polynya, Nature Geoscience, p. 1, https://www.nature.com/articles/s41561-019-0356-0, 2019.

Tamura, T., Ohshima, K. I., Nihashi, S., and Hasumi, H.: Estimation of Surface Heat/Salt Fluxes Associated with Sea Ice Growth/Melt in the Southern Ocean, SOLA, 7, 17–20, https://doi.org/10.2151/sola.2011-005, https://www.jstage.jst.go.jp/article/sola/7/0/7_0_17/_article, 2011.

Taylor, K. E., Stouffer, R. J., and Meehl, G. A.: An Overview of CMIP5 and the Experiment Design, Bulletin of the American Meteorological Society, 93, 485–498, https://doi.org/10.1175/BAMS-D-11-00094.1, https://journals.ametsoc.org/doi/10.1175/BAMS-D-11-00094.1, 2011.

Thoma, M., Jenkins, A., Holland, D. M., and Jacobs, S. S.: Modelling Circumpolar Deep Water intrusions on the Amundsen Sea continental

730   shelf, Antarctica, Geophysical Research Letters, 35, https://doi.org/10.1029/2008GL034939, https://agupubs.onlinelibrary.wiley.com/doi/abs/10.1029/2008GL034939, 2008.

Timmermann, R., Wang, Q., and Hellmer, H. H.: Ice shelf basal melting in a global finite-element sea ice/ice shelf/ocean model, Annals of Glaciology, 53, https://doi.org/10.3189/2012AoG60A156, http://www.igsoc.org/annals/53/60/t60A156.html, 2012.

Williams, G. D., Herraiz-Borreguero, L., Roquet, F., Tamura, T., Ohshima, K. I., Fukamachi, Y., Fraser, A. D., Gao, L., Chen, H., McMahon,

735   C. R., Harcourt, R., and Hindell, M.: The suppression of Antarctic bottom water formation by melting ice shelves in Prydz Bay, Nature Communications, 7, 12 577, https://doi.org/10.1038/ncomms12577, https://www.nature.com/articles/ncomms12577, 2016.